Global and Planetary Change 234 (2024) 104382

Contents lists available at ScienceDirect

Global and Planetary Change

journal homepage: www.elsevier.com/locate/gloplacha

Sediment provenance changes in the southwestern Okhotsk Sea since MIS 5 and their implications for sediment transport dynamics

Anqi Wang [a,b,c], Zhengquan Yao [b,d,*], Xuefa Shi [b,d,*], Kunshan Wang [b,d], Yanguang Liu [b,d], Jianjun Zou [b,d], Yuriy Vasilenko [f], Fengdeng Shi [b,d], Zhi Dong [b], Xiaojing Wang [b,d], Aimei Zhu [b,d], Zhengfan Lin [e], Xinqing Zou [a,c,**], Sergey Gorbarenko [f], Alexander Bosin [f]

[a] *School of Geography and Ocean Science, Nanjing University, Nanjing 210093, China*
[b] *Key Laboratory of Marine Geology and Metallogeny, First Institute of Oceanography, Ministry of Natural Resources, Qingdao 266061, China*
[c] *Collaborative Innovation Center of South China Sea Studies, Key Laboratory for Coast and Island Development, Ministry of Education, Nanjing University, Nanjing 210093, China*
[d] *Laboratory for Marine Geology, Laoshan Laboratory, Qingdao 266237, China*
[e] *State Key Laboratory for Mineral Deposits Research, Nanjing University, Nanjing 210093, China*
[f] *V.I. Il'ichev Pacific Oceanological Institute of Far East Branch of Russian Academy of Science, Vladivostok 690041, Russia*

ARTICLE INFO

Editor: Jimin Sun

Keywords:
Strontium and neodymium isotopes
Sediment provenance
Sea ice
Okhotsk Sea

ABSTRACT

The Okhotsk Sea, located between the Asian continent and the western Pacific, is a natural laboratory for investigating sediments source-to-sink influenced by atmosphere–ocean–land–sea ice interactions. However, despite their paleoenvironmental significance, changes in sediment provenance within the Okhotsk Sea are still debated due to the diversity of sediment sources and transport processes. Here, we investigate Sr and Nd isotope compositions in surface sediment samples from regions across the Okhotsk Sea, as well as Sr and Nd isotope compositions and elemental abundances in the sediments of core LV55-40-1, collected from the southwestern Okhotsk Sea. Our results reveal an increasing trend of εNd values over the past ~110 kyr, with an abrupt increase during the transition into the last deglacial/early Holocene (MIS 1). We also observed minor variations characterized by less radiogenic εNd during the glacial/stadial (G/S) periods (MIS 5d, MIS 5b, MIS 4, MIS 2), and more radiogenic εNd during the interglacial/interstadial (I/I) periods (MIS 5c, MIS 5a, MIS 3). The major terrigenous sediment sources in the northwestern Okhotsk Sea are via the Amur River and from Sakhalin Island (~60–80%), with a minor volcanic contribution (~20–40%) from the Okhotsk-Chukotka volcanic belt and the southern Kuril Islands/Hokkaido. Provenance variations are primarily controlled by the interplay of sea-ice drifting and ocean circulation, reflecting a dominant transport mode shift from sea ice to surface current dominance since the early Holocene. During the G/S periods with severe sea-ice condition, terrigenous materials from the Amur River and Sakhalin Island were transported to the study site, due to the southeastward drift of sea ice driven by the prevailing northwesterly winds and enhanced Okhotsk Sea Intermediate Water circulation. In contrast, during the I/I periods with moderate sea-ice conditions, an increased contribution from the Okhotsk-Chukotka volcanic belt was caused by sea-ice drifting southwestwards under the prevailing northerly and northeasterly winds, supplemented by surface currents. This study provides the first Sr-Nd isotopes record spanning the last glacial cycle in the Okhotsk Sea and it offers new insights into the relationship between sediment provenance and the interplay of sea ice and ocean currents in this region.

1. Introduction

Sea ice is an important component of the global climate system, and its expansion and retreat are sensitive to both local and global climate change. Sea ice significantly influences the regional climate via feedback mechanisms within the climate system (Serreze et al., 2016; Turner

* Corresponding authors at: Key Laboratory of Marine Geology and Metallogeny, First Institute of Oceanography, Ministry of Natural Resources, Qingdao 266061, China.
** Correspongding author at: School of Geography and Ocean Science, Nanjing University, Nanjing 210093, China
E-mail addresses: yaozq@fio.org.cn (Z. Yao), xfshi@fio.org.cn (X. Shi), zouxq@nju.edu.cn (X. Zou).

https://doi.org/10.1016/j.gloplacha.2024.104382
Received 1 September 2023; Received in revised form 7 February 2024; Accepted 7 February 2024
Available online 10 February 2024
0921-8181/

et al., 2015). The Okhotsk Sea, in the northwestern Pacific Ocean, is located on the southernmost boundary of sea ice influence in the north hemisphere, where the sedimentary source-to-sink process is highly sensitive to the interaction between sea ice, oceanic and atmospheric circulation. The Okhotsk Sea features a variety of sediment sources, attributable to complex ocean-land interactions (Chebykin et al., 2015; Derkachev et al., 2004; Gorbarenko et al., 2002, 2012; Nürnberg and Tiedemann, 2004; Wang et al., 2017, 2021b; Yasuda et al., 2014), sea-ice dynamics and ocean circulation (Vasilenko et al., 2017, 2019; Wang et al., 2014, 2017; Yasuda et al., 2014; Zou et al., 2015). Hence, investigating past changes in sediment provenance in the Okhotsk Sea can contribute to a better understanding of the mechanisms governing sediment transport processes in this region and their relationship with regional and global climate changes.

Sea-ice drifting plays a crucial role in regulating changes in sediment provenance in the Okhotsk Sea (Vasilenko et al., 2017, 2019; Wang et al., 2017; Zou et al., 2015). Evidence from the elemental composition of sediments from the central and southern Okhotsk Sea suggests that sea-ice rafting was the predominant sediment transport mechanism during cold intervals, while sediments supplied by the Amur River also contributed during warm intervals (Nürnberg and Tiedemann, 2004; Zou et al., 2015). Mineralogical studies of the clastic materials of the Okhotsk Sea indicate that the coast of West Kamchatka was the main source of ice-rafted debris (IRD) in the eastern Okhotsk Sea during the last glaciation (Derkachev et al., 2004; Vasilenko et al., 2017), while Nürnberg et al. (2011) showed that IRD was discharged by icebergs from the coast of southern Kamchatka during Marine Isotope Stage (MIS) 3. Furthermore, Wang et al. (2017) investigated the distribution and sources of clastic minerals in the southern Okhotsk Sea and revealed a clastic materials transition from the eastern Okhotsk Sea to the northeastern region between cold and warm stages, driven by changes in sea-ice drifting. The existing research on sea-ice drifting and its changes in provenance over geological timescales has primarily concentrated on the coarse fractions of IRD. However, there is a noticeable gap in the study of finer fractions. Additionally, the majority of these studies have been centered around the central and eastern regions of the Okhotsk Sea, with limited research conducted in the western Okhotsk Sea. Moreover, previous studies suggested that in addition to sea ice, the sediments in this region could also be transported by the surface and intermediate-depth ocean currents (Derkachev et al., 2004; Nakatsuka et al., 2002; Nakatsuka, 2004; Yasuda et al., 2014). However, the evolution of sediment sources and the linked transport processes in the southwestern Okhotsk Sea over glacial-interglacial cycles are still not well understood, mainly due to the scarcity of well-dated sedimentary records with suitable provenance proxies.

The isotopes of strontium (Sr) and neodymium (Nd) have been widely used to discriminate the provenance of marine sediments (Asahara et al., 2012; Dou et al., 2012; Frank, 2002; Li et al., 2015; Tütken et al., 2002; Yao et al., 2023; Zou et al., 2021). In this study, we analyzed the Sr-Nd isotopic compositions of the detrital components of surface sediments from the Okhotsk Sea, and of sediment core LV55-40-1 from the southwestern Okhotsk Sea, to investigate provenance changes. Our findings reveal the history of provenance changes and the underlying mechanisms, highlighting the interplay between sea ice and ocean currents in the Okhotsk Sea since the last interglacial period.

2. Regional setting

The Okhotsk Sea is the second largest marginal sea in the Pacific Ocean, with an area of 1.59 $\times$ 10^6 km^2 and an average water depth of 838 m (Lapko and Radchenko, 2000). It was formed during the Miocene, at the site of the Late Cretaceous volcanic arc and marginal basin within this region (Savostin et al., 1983). The Okhotsk Sea is surrounded by a series of volcanic belts and island arcs (Lapko and Radchenko, 2000), including the Okhotsk-Chukotka volcanic belt adjacent to the northern Okhotsk Sea, the Kamchatka volcanic belt in the eastern part of the Okhotsk Sea, and the southern Kuril Islands/Hokkaido in the southern Okhotsk Sea (Fig. 1). The western Okhotsk Sea is bordered by Sakhalin Island and connected to the Japan Sea via the Tatar Strait and Soya Strait, and its southeastern part is connected to the northwest Pacific Ocean via the Kruzenshterna Strait and Bussol Strait (Fig. 1).

The Okhotsk Sea is located on the southernmost boundary of the region of sea-ice-influence and approximately two-thirds of the Okhotsk Sea is covered by sea ice during winter (Sakamoto et al., 2006). Sea ice forms on the northern coast of the Okhotsk Sea in November and reaches its maximum coverage in the following March, due to the influence of the winter winds (Rycroft, 1995). Sea ice disappears entirely in June, and ice-free conditions are maintained from July to October (Parkinson et al., 1987).

The Amur River is the largest river entering the Okhotsk Sea, with an average annual runoff of ~7–14 $\times$ 10^3 m^3/s. The sediment flux of the Amur River (5.2 $\times$ 10^7 ton/a; Meade, 1996) is 2–3 times higher than those of all other Siberian rivers. Therefore, sediment input from the Amur River has a large impact on sedimentation in the Okhotsk Sea. Due to the influence of the modern circulation, most of the terrigenous material transported by the Amur River is deposited near Sakhalin Island, while fine particles can be transported to the southern Okhotsk Sea (Yasuda et al., 2014; Zou et al., 2015).

The surface circulation in the Okhotsk Sea is characterized by a cyclonic gyre composed of the West Kamchatka Current (WKC), the Sredinnoe Current (SC), and the East Sakhalin Current (ESC). The WKC is driven by relatively warm, highly saline Pacific water entering the Okhotsk Sea via the Kruzenshterna Strait (Talley, 1991; Wong et al., 1998), and flows northward along the western Kamchatka Peninsula; it then turns to southward as the ESC, along the eastern part of Sakhalin Island to the Kuril Islands, and eventually flows out of the Okhotsk Sea, mainly through the Bussol Strait (Lapko and Radchenko, 2000). Additionally, a gyre called the Northeast Current (NC) forms in the western and central parts of the Kuril Basin affected by the high-salinity Soya Warm Current (SWC) through the Soya Strait, transporting the fine volcanic materials from the southern Kuril Islands/Hokkaido. In addition to the surface circulation, the Okhotsk Sea also develops the Okhotsk Sea Intermediate Water (OSIW), at depths of 300–800 m and characterized by relatively low-density (26.7–27$\sigma\theta$), low-salinity (33.8‰), and oxygen-rich water (Morley and Hays, 1983; Talley, 1991, 1993; Yang and Honjo, 1996), while CO_2-enriched water masses from the deep Pacific occur below the OSIW (Nürnberg and Tiedemann, 2004). The characteristics of the OSIW are similar to the North Pacific Intermediate Water (NPIW) and it is regarded as the present-day source of the NPIW (Freeland et al., 1998; Talley, 1991; Wong et al., 1998; Yasuda, 1997).

3. Materials and methods

Sediment core LV55-40-1 (48.12°N, 147.15°E, 1730 m depth) was recovered from the southwestern Okhotsk Sea during the Chinese-Russian expedition aboard R/V “Akademik M.A. Lavrentiev”, cruise LV55 in 2011 (Fig. 1). The 8.8 m-long core is composed of olive-gray silty clay with two distinct layers of coarse-grained sand and gravels at the depths of 340–345 cm and 385–388 cm, respectively. The age model of core LV55-40-1 is based on AMS ^{14}C dating of planktonic foraminifera and the correlation of productivity proxies (Ba/Ti, chlorin, and opal contents) with the standard marine oxygen isotope record. The basal age is ~110 ka (Wang et al., 2021a). Seven surface sediment samples were obtained during Chinese-Russian expeditions aboard R/V Akademik M.A. Lavrentiev cruise LV55 (in 2011) and LV87 (in 2019).

Twenty-seven bulk sediments samples from core LV55-40-1 and 7 surface samples from the Okhotsk Sea were collected for Sr-Nd isotopic analysis. Before analysis, carbonates and organic matter were removed with 0.25 N acetic acid and 5% H_2O_2, respectively. Approximately 200 mg of sample was dissolved in a Teflon beaker with a mixture of ultrapure 1.5 mL HF-1 mL HNO_3-3 mL HCl. Sr and Nd isotopes were

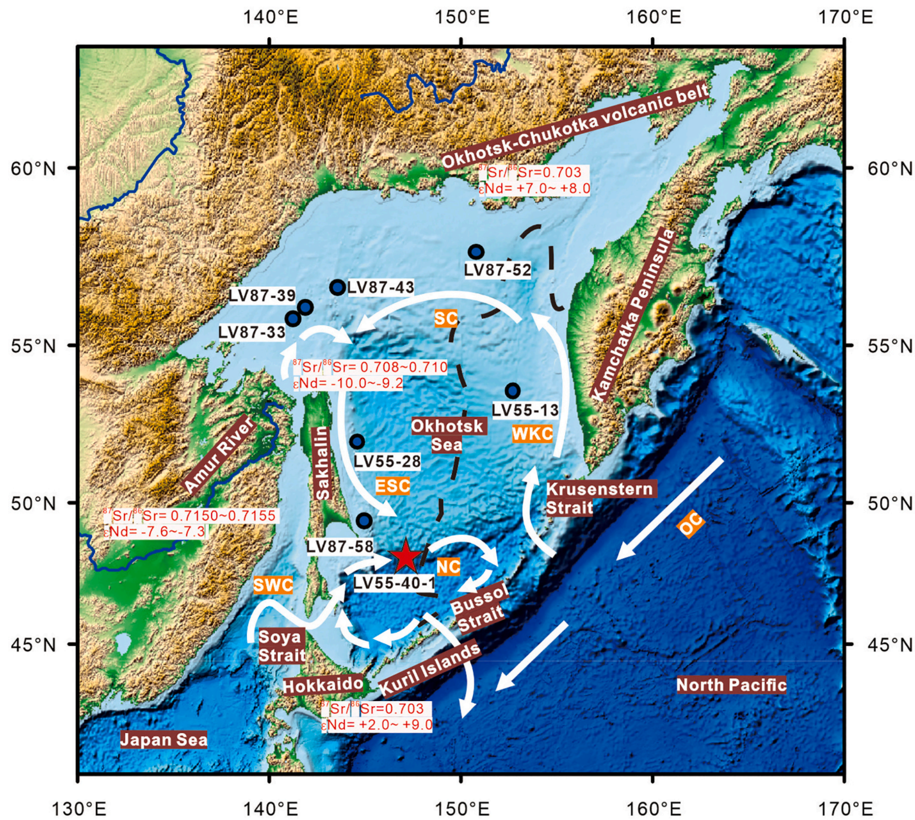

Fig. 1. Map showing general information about the Okhotsk Sea and the locations of core LV55-40-1 (red star), and surface sediment sampling sites LV55-13, LV55-28, LV87-33, LV87-39, LV87-43, LV87-52, and LV87-58 (blue dots). White arrows represent the East Sakhalin Current (ESC), West Kamchatka Current (WKC), Soya Warm Current (SWC), Sredinnoe Current (SC), Northeast Current (NC) and Oyashio Current (OC). The dashed line represents the average sea-ice boundary from November to June, according to Lo et al. (2018). The average values of the Sr and Nd isotopes for the geologic provinces around the Okhotsk Sea are from the GEOROC database (http://georoc.mpch-mainz.gwdg.de/georoc/), Churikova et al. (2001), Horikawa et al. (2010), Martynov et al. (2007) and Shuto et al. (2004). (For interpretation of the references to colour in this figure legend, the reader is referred to the web version of this article.)

separated and extracted using an ion chromatography column at the State Key Laboratory for Mineral Deposits Research at Nanjing University. Briefly, Sr was separated with 0.05 N HNO_3 using Sr-spec resin, and Nd was extracted with 0.25 N HCl with LN resin. Sr and Nd isotopes were measured using a MC-ICP-MS (Thermo Fisher NEPTUNE plus). To monitor the quality of the measurements, NBS 987 and JNdi-1 standards were included with every five samples to assess the accuracy of measurements. The obtained Sr and Nd isotopes ratios were normalized to NBS987 = 0.710245 (Steiger and Jäger, 1977) and JNdi-1 = 0.512115 (Tanaka et al., 2000), respectively. Repeat measurement of standard sample JG-2 yielded $^{87}Sr/^{86}Sr$ = 0.708813 and $^{143}Nd/^{144}Nd$ = 0.512248, respectively. Nd results are expressed as $\varepsilon Nd = [(^{143}Nd/^{144}Nd\ (measured)/^{143}Nd/^{144}Nd\ (CHUR)) - 1] \times 10^4$, with the CHUR value of 0.512638 (Jacobsen and Wasserburg, 1980).

A total of 220 samples at ~4 cm intervals were analyzed for elemental abundance using a modified pretreatment procedure (Chen et al., 2021; Dou et al., 2022). Briefly, carbonates and organic matter were removed before analysis. Then, ~50.00 mg (49.50–50.50 mg) of sediment was digested in a Teflon beaker with a mixture of high-purity HNO_3 and HF. Trace elements and rare earth elements (REEs) were analyzed on a Thermal series II ICP-MS. Quality control during analysis was monitored with GSD-9, duplicate samples, and blank samples. The relative standard deviations of trace elements and REEs analysis were <5%.

The end-member (EM) analysis of sediment grain-size distribution is an effective method for distinguishing different provenances or transport mechanisms (Weltje, 1997). We analyzed the grain size data of core LV55-40-1 (Wang et al., 2021a) to calculated the mean complex correlation coefficient (R^2 mean) of the grain size distributions, assuming five end-members (Fig. 4A). The respective R^2 mean values are 89.7%, 96.7%, 98.6%, 99.2%, and 99.7% for end-members (EM) 1–5 (Fig. 4A). Based on the grain size data, we used four end members to retrieve the varying contributions of the end-members (Fig. 4B).

4. Results

4.1. Sr and Nd isotopic compositions

The Sr-Nd isotopic compositions of the surface sediments and samples from core LV55-40-1 are presented in Tables 1 and 2, respectively. The εNd values of the surface sediments range from −5.4 to 2.7 with the mean of −1.6. For the surface sediments, the εNd values are higher at sites LV87-52 (εNd: 1.6) and LV55-13 (εNd: 2.7), near the northeastern shelf and the Kamchatka Peninsula, and the lowest values are at sites LV55-28 (εNd: −5.0) and LV87-58 (εNd: −5.4) off eastern Sakhalin Island; intermediate values occur at sites LV87-43, LV87-39, and LV87-33, from near the northwestern shelf, with the mean of −1.7 (Fig. 2A). The εNd values of the surface sediments show a generally decreasing trend (except the core-top sample of LV55-40-1) from the northeastern region to the southwestern region of the Okhotsk Sea, with higher values close to the Kamchatka Peninsula and the northeastern shelf, and lower εNd values occur closed to eastern Sakhalin Island (Fig. 2A). The $^{87}Sr/^{86}Sr$ ratios range from 0.705671 to 0.708813 with the mean of 0.706648, and the spatial distribution shows the opposite pattern to that of the εNd

Table 1
Sr-Nd isotopic compositions of surface sediment samples from the Okhotsk Sea.

Station	Latitude (°)	Longitude (°)	$^{87}Sr/^{86}Sr$	2σ	$^{143}Nd/^{144}Nd$	2σ	εNd	2σ
LV55-13	53.61	152.73	0.705671	0.000005	0.512775	0.000004	2.7	0.07
LV55-28	52.00	144.63	0.707025	0.000005	0.512380	0.000003	−5.0	0.05
LV87-33	55.80	141.25	0.706577	0.000005	0.512518	0.000004	−2.3	0.08
LV87-39	56.13	141.89	0.706498	0.000004	0.512600	0.000003	−0.7	0.05
LV87-43	56.70	143.54	0.705757	0.000007	0.512531	0.000003	−2.1	0.06
LV87-52	57.70	150.79	0.706199	0.000005	0.512720	0.000005	1.6	0.09
LV87-58	49.40	144.94	0.708813	0.000005	0.512359	0.000007	−5.4	0.14

Table 2
Sr-Nd isotopic compositions, Th/Sc ratio, and mean grain size of sediments for core LV55-40-1 from the southwestern Okhotsk Sea.

Age (ka)	$^{87}Sr/^{86}Sr$	2σ	$143_{Nd}/144_{Nd}$	2σ	εNd	2σ	Sr (μg/g)	Nd (μg/g)	Th/Sc	Mz (μm)
1.1	0.708538	0.000005	0.512474	0.000003	−3.2	0.05	110.27	8.59	0.60	3.98
5.0	0.708777	0.000005	0.512469	0.000017	−3.3	0.33	175.62	13.10	0.55	3.40
7.2	0.708053	0.000005	0.512477	0.000003	−3.1	0.06	186.26	14.37	0.54	3.87
10.0	0.708496	0.000005	0.512428	0.000003	−4.1	0.07	220.07	16.41	0.57	5.73
15.2	0.709013	0.000005	0.512458	0.000006	−3.5	0.12	199.08	17.79	0.61	6.71
19.2	0.709203	0.000003	0.512398	0.000002	−4.7	0.05	185.88	17.69	0.66	5.21
22.7	0.709228	0.000016	0.512394	0.000004	−4.8	0.07	190.63	15.60	0.74	6.90
25.0	0.709981	0.000005	0.512409	0.000004	−4.5	0.08	175.00	17.36	0.82	5.08
27.4	0.706640	0.000006	0.512727	0.000003	1.7	0.05	163.66	14.67	0.55	7.73
29.1	0.708191	0.000012	0.512419	0.000005	−4.3	0.10	180.70	13.21	0.48	8.81
31.5	0.704441	0.000006	0.512881	0.000004	4.7	0.08	212.38	10.32	0.13	7.32
35.6	0.709628	0.000009	0.512387	0.000004	−4.9	0.08	184.07	15.46	0.71	5.28
40.7	0.709226	0.000005	0.512429	0.000002	−4.1	0.04	188.22	14.89	0.77	6.97
55.5	0.709555	0.000011	0.512390	0.000006	−4.8	0.11	197.24	17.15	0.70	6.90
60.7	0.709489	0.000005	0.512382	0.000004	−5.0	0.08	200.48	16.81	0.70	7.80
68.2	0.709776	0.000011	0.512403	0.000005	−4.6	0.09	182.89	19.26	0.72	5.41
70.7	0.709906	0.000010	0.512402	0.000004	−4.6	0.08	173.61	18.41	0.71	6.24
75.3	0.710095	0.000012	0.512370	0.000004	−5.2	0.09	180.29	17.31	0.71	6.80
80.0	0.709302	0.000009	0.512387	0.000005	−4.9	0.09	183.98	16.06	0.73	6.02
83.2	0.709040	0.000008	0.512399	0.000004	−4.7	0.09	187.09	15.48	0.66	6.30
86.1	0.709937	0.000008	0.512340	0.000005	−5.8	0.10	183.40	17.77	0.74	7.72
88.7	0.709585	0.000009	0.512332	0.000005	−6.0	0.09	180.34	17.91	0.83	6.36
91.8	0.709818	0.000006	0.512439	0.000004	−3.9	0.08	189.70	17.74	0.75	7.70
95.7	0.709063	0.000008	0.512397	0.000004	−4.7	0.09	203.15	15.89	0.65	8.31
100.7	0.709180	0.000011	0.512370	0.000005	−5.2	0.09	200.16	16.15	0.80	6.73
104.8	0.709209	0.000004	0.512345	0.000004	−5.7	0.07	202.06	16.71	0.71	6.04
109.0	0.709700	0.000008	0.512365	0.000004	−5.3	0.08	197.15	17.88	0.75	5.77

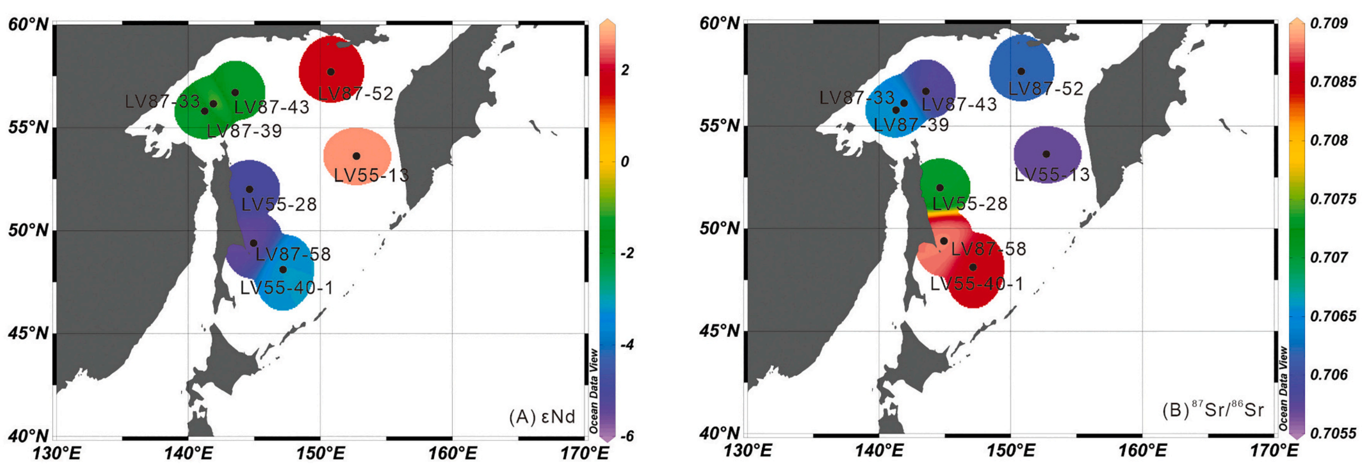

Fig. 2. Sr and Nd isotopic compositions of surface sediments in the Okhotsk Sea. (A) εNd values and (B) $^{87}Sr/^{86}Sr$ ratio.

values (Fig. 2B).

The εNd values of core LV55-40-1 vary widely, from −6.0 to 4.7 (Fig. 3E), with the mean of −4.0 (Table 2 and Fig. 3E). The εNd values show a prominent increasing trend, with an abrupt increase in εNd values occurring in the last deglacial/early Holocene transition (MIS 1; Fig. 3E). Superimposed on this increasing trend, there are secondary cyclic fluctuations, with more radiogenic values occurring during the interglacial/interstadial (I/I) periods (MIS 5c, MIS 5a, MIS 3), and less radiogenic values during the glacial/stadial (G/S) periods (MIS 5d, MIS 5b, MIS 4, MIS 2; Fig. 3A, E). In contrast to the variation of the εNd values, the $^{87}Sr/^{86}Sr$ ratios, which range from 0.704441 to 0.710095, are less radiogenic during the I/I periods (Table 2 and Fig. 3F). In

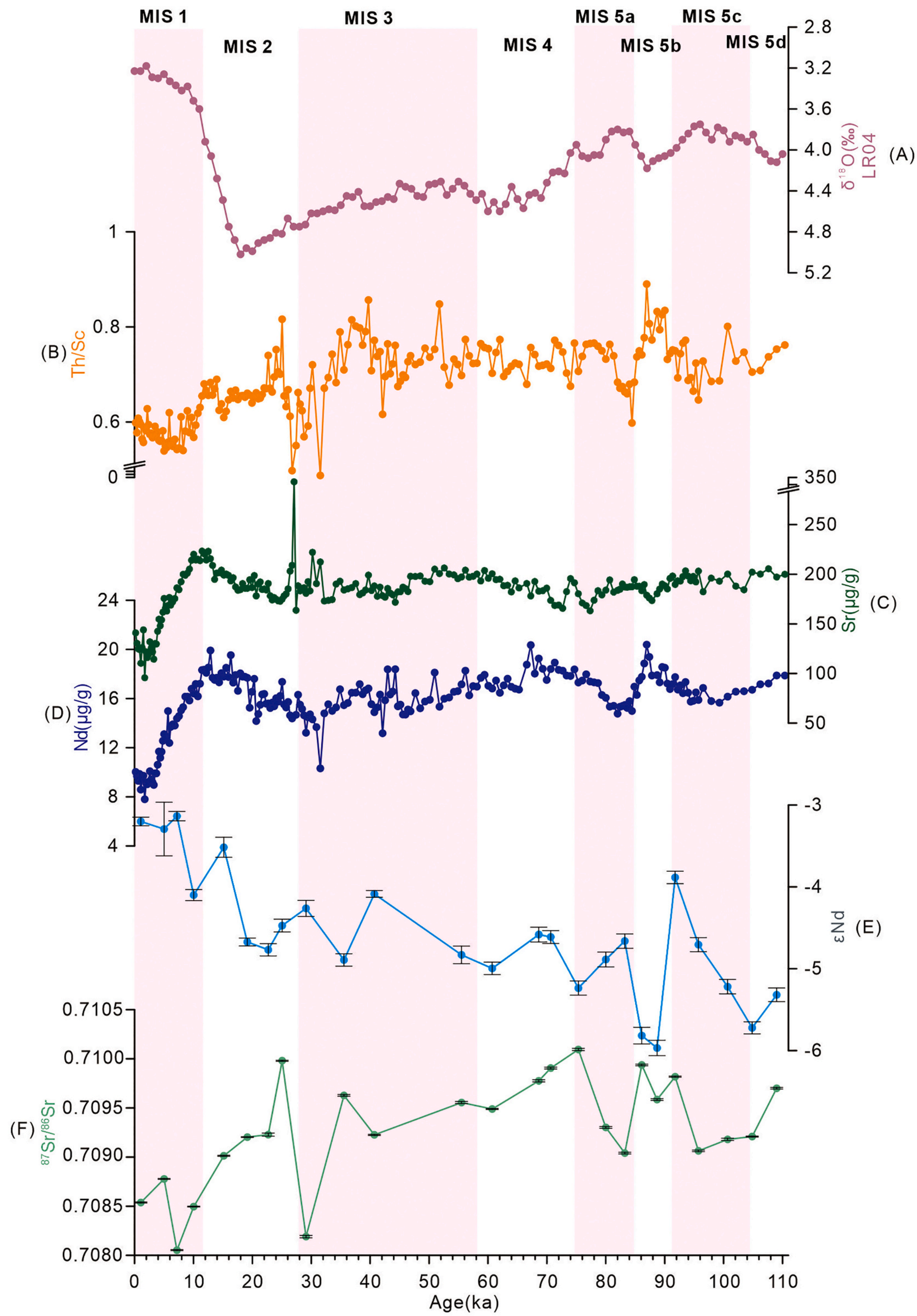

Fig. 3. Variations in geochemical proxies of core LV55-40-1. (A) LR04 marine oxygen isotope stack (Lisiecki and Raymo, 2005) with marine isotope stages (MIS) indicated, (B) Th/Sc ratio, (C) Sr concentration, (D) Nd concentration, (E) εNd values, and (F) $^{87}Sr/^{86}Sr$ ratio, both with 2σ error bars. The εNd values (1.74 and 4.74) and $^{87}Sr/^{86}Sr$ ratios (0.706640 and 0.704441), corresponding to the volcanic layers at ~27.4 ka and ~ 31.5 ka, are not shown in the figure. The pink bars represent the interglacial/interstadial (I/I) periods (MIS 5c, MIS 5a, MIS 3) and the Holocene. (For interpretation of the references to colour in this figure legend, the reader is referred to the web version of this article.)

general, the variations of εNd and $^{87}Sr/^{86}Sr$ are negatively correlated throughout core LV55-40-1. Several abrupt changes in εNd values are evident, such as the elevated values during mid-MIS 4 (~68 ka) and during the deglacial period (~15 ka), with lower values in mid-MIS 3 (~36 ka) and the early Holocene (~10 ka; Fig. 3E); we interpret these changes as representing abrupt climate events. Additionally, two notably high εNd values, corresponding to the least radiogenic $^{87}Sr/^{86}Sr$ ratios, occurred at ~31.5 ka and ~ 27.4 ka (Table 2).

4.2. Elemental concentrations

The Nd concentrations in the sediments of core LV55-40-1 vary between 7.80 μg/g and 20.38 μg/g, with the mean of 15.78 μg/g (Fig. 3D). Contrary to the variations in Nd isotopes, there is a concurrent decrease in Nd concentration (Fig. 3D, E). The Nd content is lower during the I/I periods, while a higher Nd content occurred during the G/S periods, except for the abrupt decrease in Nd concentration at ~31.4 ka (Fig. 3D). The Sr concentrations range from 95.69 to 319.64 μg/g, with the mean of 184.15 μg/g, and they show a similar temporal pattern to that of the Nd content. Two peaks in Sr concentration occurred at ~31.5 ka and ~ 27.4 ka, respectively (Fig. 3C). The elemental ratio of Th/Sc ranges from ~0.13 to ~0.89 with the mean of 0.68; lower values occurred during the I/I periods, with a generally decreasing trend (Fig. 3B), which is negatively correlated to the variations in εNd during the past ~110 kyr (Fig. 3E). Two especially low Th/Sc ratios occurred at ~31.5 ka and ~ 27.4 ka, respectively, corresponding to the abrupt changes in Sr-Nd isotopes and concentrations (Fig. 3B and Table 2).

4.3. End-member analysis of the sedimentary grain-size distributions of core LV55-40-1

EM1 has the grain size range of 0.22–57.8 μm, with the mean (Mz) of 1.76 μm, representing the finest fraction; these sediments are predominantly clay (~81%) and silt (~19%) (Fig. 4B). The EM1 content varies between ~0.5% and ~ 51%, with the highest content during the Holocene (Fig. 5B). This finest EM may be sensitive to surface ocean currents (McCave, 2008; Sakamoto et al., 2005). EM2 has the grain size range of 1.07–115 μm (Mz = 6.62 μm) and is mainly composed of silt and clay, overlapping with EM1 and EM3 (Fig. 4B); its abundance ranges from ~2% to ~64%, with higher abundances during MIS 5c, MIS 3, MIS 2, and MIS 1 (Figs. 4B and 5C). We infer that EM2 is influenced by both ocean currents and sea ice. EM3 has the broad grain size range of 1.51–650.9 μm (Mz = 45.96 μm) and is predominantly composed of silt

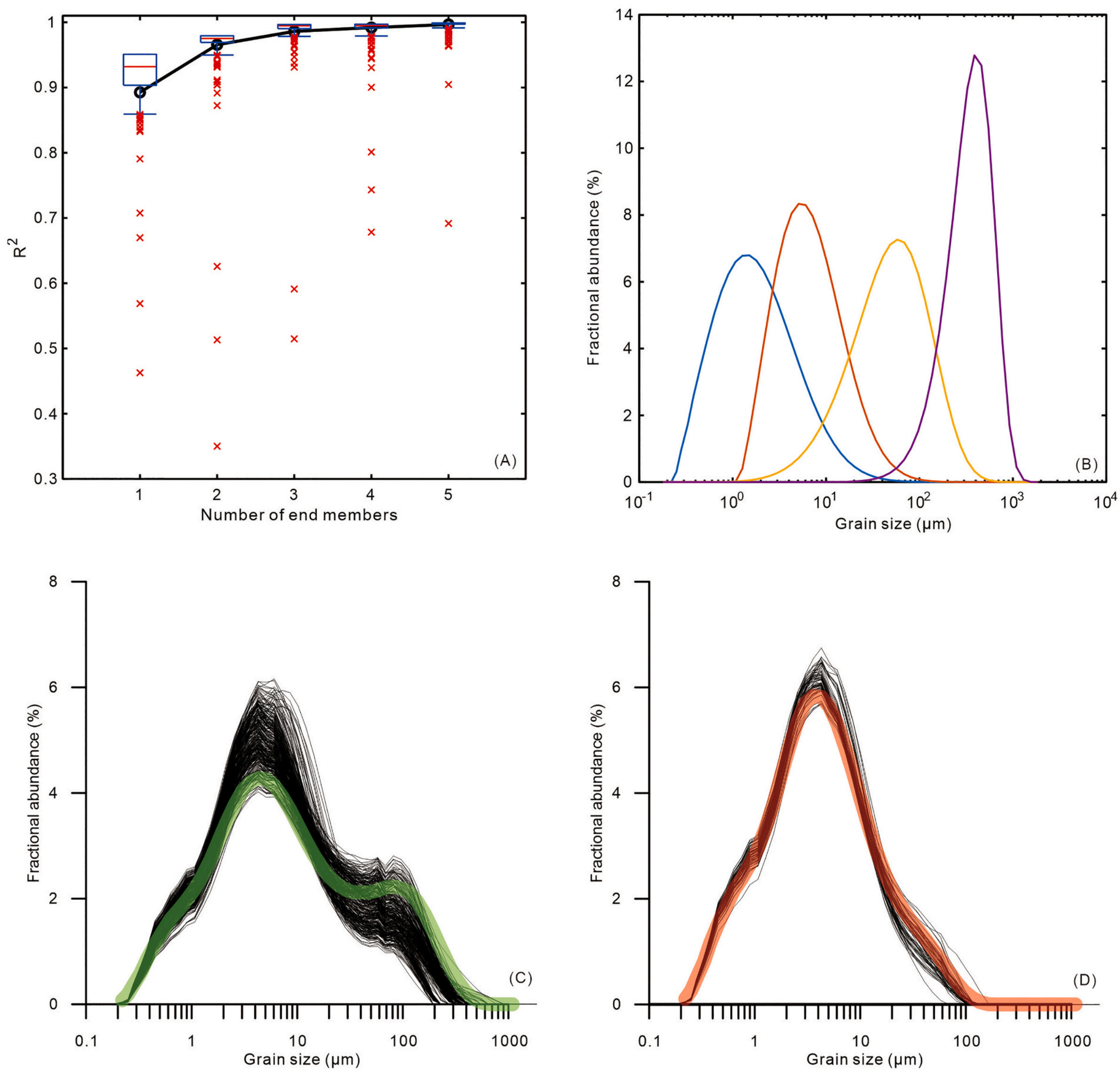

Fig. 4. Grain size analysis results for the sediments from core LV55-40-1. (A) Correlation of grain size end-members 1–5. (B) Grain-size distributions of the selected four end-members. (C) Bimodal grain-size distribution of sediments during MIS 5–2. (D) Unimodal distribution of sediments during the Holocene. Green and red bold lines represent the means values of the grain-size distributions. (For interpretation of the references to colour in this figure legend, the reader is referred to the web version of this article.)

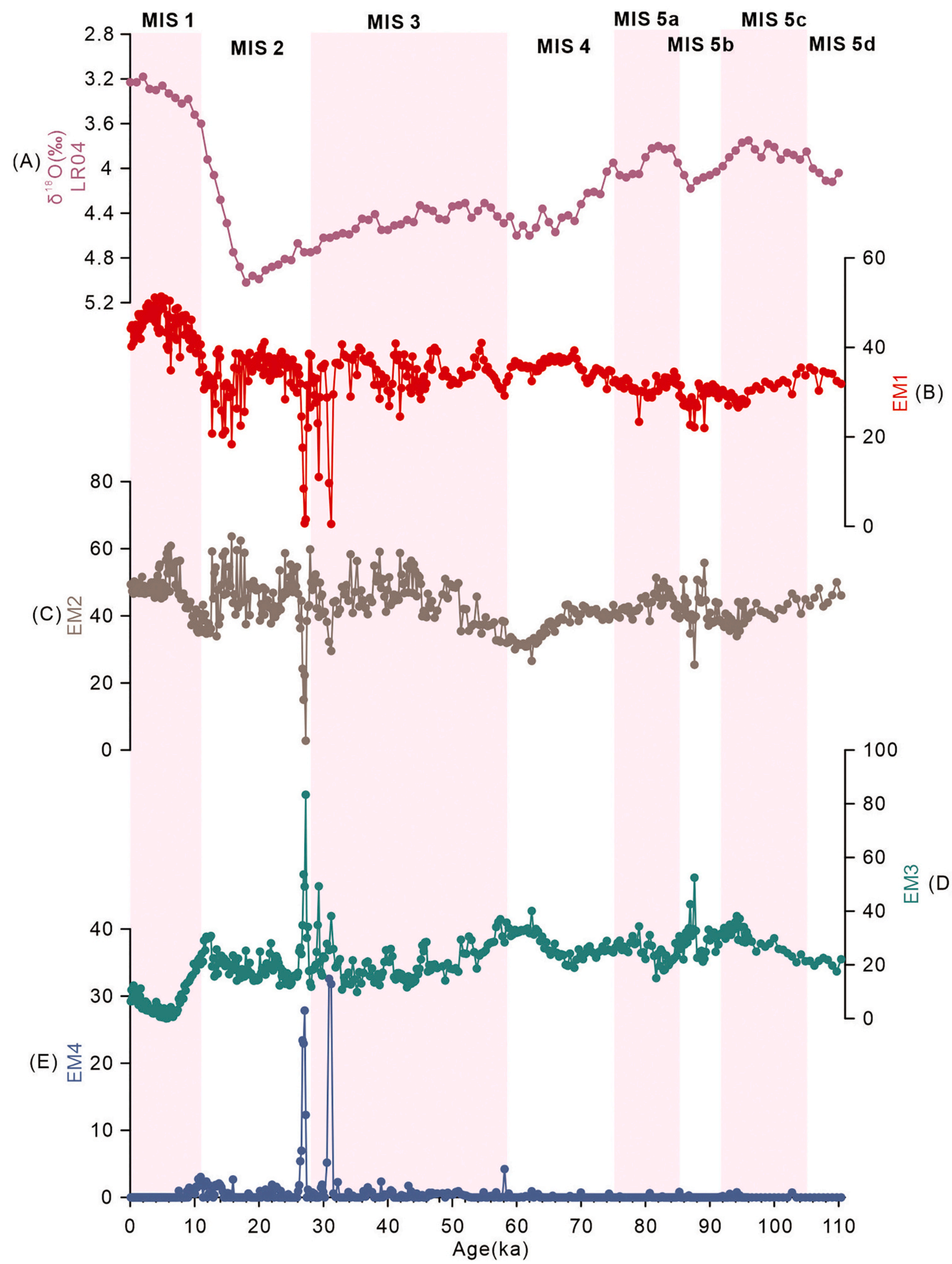

Fig. 5. Variations in the selected four grain-size end-members (EMs) in core LV55-40-1. (A) LR04 marine oxygen isotope stack (Lisiecki and Raymo, 2005) with marine isotope stages (MIS) indicated, (B) EM1, (C) EM2, (D) EM3, (E) EM4. Pink bars represent the interglacial/interstadial (I/I) periods (MIS 5c, MIS 5a, MIS 3) and the Holocene. Note that significantly high values of EM3 and EM4 correspond to volcanic layers. (For interpretation of the references to colour in this figure legend, the reader is referred to the web version of this article.)

(~62%) and sand (~38%). EM3 is linked to variations in sea ice conditions (Wang et al., 2021a; Figs. 4B and 5D). Its abundance varies from ~0% to ~83%, with high abundances observed during MIS 5b, MIS 4, and MIS 2. Notably, there is an abrupt decline in EM3 during the last deglacial/early Holocene transition, which exhibits a negative correlation with EM1 (Fig. 5D). EM4 has the grain size range of 24.19–1302 μm (Mz = 327.86 μm) and is mainly composed of sand (99%). Peaks in EM4 occurred at ~31.5 ka and ~ 27.4 ka, corresponding to abrupt changes in Sr and Nd isotopes, elemental abundances, and extremely high values of magnetic susceptibility and sand content, suggesting a possible volcanic source (Wang et al., 2021a; Figs. 4B and 5E).

5. Discussion

5.1. Changes in sediment provenance in the Okhotsk Sea since ~110 ka

The Sr and Nd isotopic compositions of the detrital components in sediments depend on the source rock compositions and thus they are widely used to trace the provenance of marine sediments (Asahara et al., 2012; Li et al., 2015; Mahoney, 2005). It is generally acknowledged that the Nd isotopic compositions of detrital materials remain stable during transport processes (McLennan, 1989; Norman and Deckker, 1990). However, Sr isotopic compositions can be influenced by grain-size sorting and chemical weathering (Colin et al., 2006; Erel et al., 1994). Generally, the mineral composition of the coarse fraction of sediments is dominated by quartz and feldspars, resulting in low $^{87}Sr/^{86}Sr$ values (Lupker et al., 2013), whereas $^{87}Sr/^{86}Sr$ is higher in fine-grained sediments due to the enrichment of clay minerals and micas (Tütken et al., 2002). However, there is no significant correlation between the $^{87}Sr/^{86}Sr$ ratio and the mean grain size of the sediments of core LV55-40-1 ($R^2 = 0.05$; Fig. 6A), suggesting that grain size effects on the Sr isotopic compositions are negligible. The R^2 value for the correlation between εNd and mean grain size is 0.18, indicating that the influence of grain size on εNd is also negligible (Fig. 6B). Moreover, the negative correlation between $^{87}Sr/^{86}Sr$ and εNd ($R^2 = 0.36$) implies that the variations in the Sr and Nd isotopic compositions in core LV55-40-1 mainly reflect changes in sediment provenance (Fig. 6C).

We carefully evaluated the potential sediment sources in core LV55-40-1 based on the regional geological background. The volcanic complexes in the Okhotsk Sea comprise the Okhotsk-Chukotka volcanic belt, the Kamchatka volcanic belt, and the southern Kuril Islands/Hokkaido (Lapko and Radchenko, 2000; Fig. 1). As sea-ice drifting from the eastern coast of the Okhotsk Sea does not extend to the southwestern area beyond ~150°E (Derkachev et al., 2004; Vasilenko et al., 2019), the primary potential sediment source in the northwestern Okhotsk Sea is the volcanic rocks in the Okhotsk-Chukotka volcanic belt and the southern Kuril Islands/Hokkaido. In these regions, the volcanic complexes are predominantly composed of andesitic-basalt, andesites, ignimbrite fields, and a small amount of rhyolite (Horikawa et al., 2010; Martynov et al., 2007; Shuto et al., 2004). The average Sr isotopic composition of sediments in the Okhotsk-Chukotka volcanic belt is ~0.703, and the average εNd of sediments from this region ranges from around +7.0 to +8.0, while that from the southern Kuril Islands/Hokkaido ranges from around +2.0 to +9.0 (Churikova et al., 2001; Horikawa et al., 2010; Martynov et al., 2007; Shuto et al., 2004; GEOROC database: http://georoc.mpch-mainz.gwdg.de/georoc/). The next potential sediment source is from the Amur River; the sediments transported by the Amur River are mostly deposited on the northwestern shelf of the Okhotsk Sea especially in the Sakhalin Bay (Wang et al., 2017, 2021b; Yasuda et al., 2014; Zou et al., 2015). These sediments primarily originate from the erosional products of early Paleozoic and early Mesozoic granitoids, as well as metamorphic rocks, with similar chemical compositions to the upper continental crust (Sorokina and Zarubina, 2011). The $^{87}Sr/^{86}Sr$ and εNd values of the suspended sediments in the Amur River range from 0.7150 to 0.7155, and from −7.6 to −7.3, respectively (Yasuda et al., 2014; Fig. 1). The other potential source is from Sakhalin Island, the northern part of which is predominantly composed of sandy sedimentary rocks formed by the ancient Amur River during the Miocene–Pliocene (Kameda et al., 2000; Oka, 1990). The $^{87}Sr/^{86}Sr$ ratios in the shelf sediments along the northeast coast of Sakhalin Island range from 0.708 to 0.710, while εNd values range between −10.0 and − 9.2 (Yasuda et al., 2014; Fig. 1).

These sediments provenances are clearly reflected in the Sr and Nd isotopic compositions of the surface sediments of the Okhotsk Sea. The Nd isotopic values of the surface sediments (samples LV87-52 and LV55-13) in the northeastern shelf are closer to the values of the Okhotsk-Chukotka volcanic belt and the Kamchatka volcanic belt (Figs. 1 and 2). Therefore, the surface sediments in the northeastern Okhotsk Sea are significantly influenced by volcanic materials from the Okhotsk-Chukotka/Kamchatka volcanic belt. The intermediate radiogenic εNd values from the surface sediments in the northwestern Okhotsk Sea (samples LV87-43, LV87-39, LV87-33) are considered to comprise a mixture of volcanic materials from the Okhotsk-Chukotka volcanic belt and terrigenous materials from the Amur River and Sakhalin Island (Figs. 1 and 2). The less radiogenic εNd values at sites LV55-28 and LV87-58 near eastern Sakhalin Island are interpreted to result from the addition of terrigenous materials from the Amur River and Sakhalin Island (Figs. 1 and 2). Furthermore, the εNd value of the core-top sediment of core LV55-40-1 is more radiogenic (~ − 3.2) than that of the surface sediments from sites LV55-28 and LV87-58 (Fig. 2), suggesting that the present-day sediment supply in the study area is less influenced by Sakhalin Island, as the materials transported from Sakhalin Island towards the offshore region are very limited compared to the shelf sediments along the eastern coast of Sakhalin Island (Wang et al., 2021b; Yasuda et al., 2014), and there is an additional contribution from the southern Kuril Islands/Hokkaido through the NC (Petelin, 1957).

By integrating the $^{87}Sr/^{86}Sr$ and εNd values from the surface sediments and core samples, we generated a discrimination plot of $^{87}Sr/^{86}Sr$ vs. εNd. The relative contribution from the potential sediment sources was obtained using a three end-member mixing model (Fig. 7). This enabled us to infer provenance changes of the terrigenous materials in the Okhotsk Sea over the past ~110 kyr, and to quantitatively estimate the contribution of volcanic and terrigenous sources (Fig. 7). The Sr and Nd isotopic compositions of the sediments in core LV55-40-1 since MIS 5 are aligned along the mixing curve linking materials from the Amur River and Sakhalin Island (with less radiogenic εNd), and from the Okhotsk-Chukotka volcanic belt and the southern Kuril Islands/Hokkaido (with more radiogenic εNd) (Fig. 7A). These results suggest that the sediments in the study area since MIS 5 are a mixture of provenances, with the major contribution (~60–80%) from the Amur River and Sakhalin Island, and a minor contribution (~20–40%) from the Okhotsk-Chukotka volcanic belt and the southern Kuril Islands/Hokkaido. Close examination reveals a minor increase of ~10–20% in the relative contribution of sediments from the Okhotsk-Chukotka volcanic belt and the southern Kuril Islands/Hokkaido during the I/I periods, compared to the G/S periods (Fig. 7A, B).

Additionally, fine-grained eolian dusts may have been supplied to

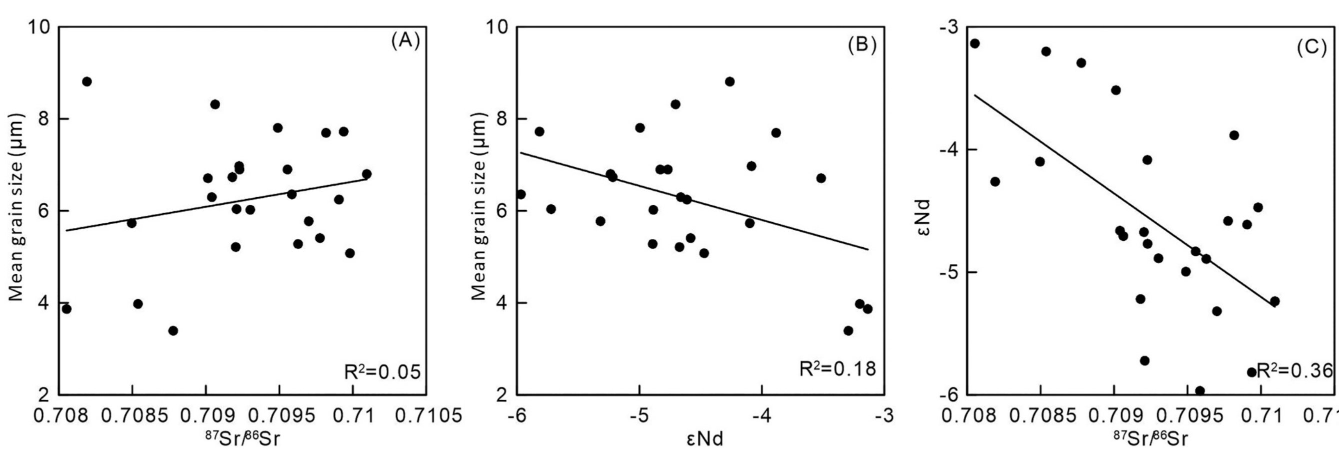

Fig. 6. Scatter plots of Sr-Nd isotopes versus grain size of core LV55-40-1. (A) $^{87}Sr/^{86}Sr$ versus mean grain size, (B) εNd versus mean grain size, and (C) $^{87}Sr/^{86}Sr$ versus εNd.

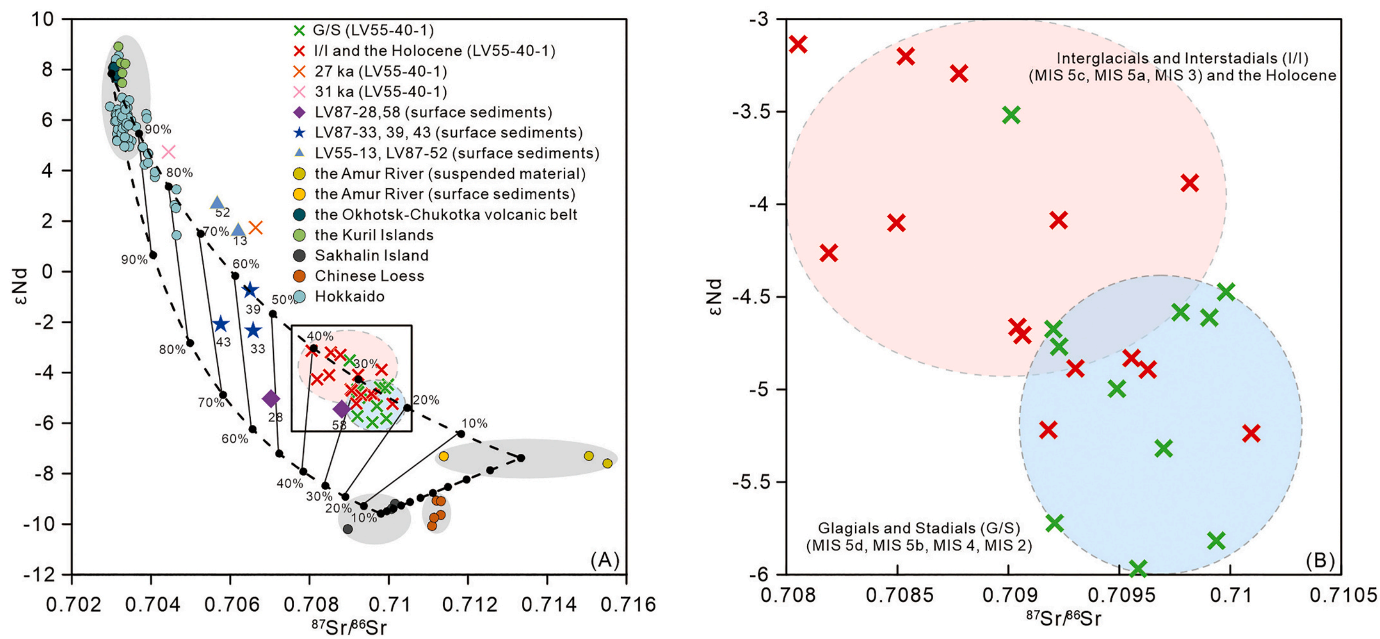

Fig. 7. Discrimination of sediment provenances in core LV55-40-1 and the surface sediment samples. (A) $^{87}Sr/^{86}Sr$ versus εNd diagram for core LV55-40-1 and the potential sediments sources of the Amur River and Sakhalin Island (Yasuda et al., 2014), the Okhotsk-Chukotka volcanic belt (Apt et al., 1998; Tschegg et al., 2011), the southern Kuril Islands/Hokkaido (Martynov et al., 2007), Hokkaido (Shuto et al., 2004), and eolian dusts from the Chinese Loess Plateau (Xie et al., 2019). (B) Enlarged plot of the Sr-Nd data from panel (A). The pink shading indicates the interglacial/interstadial (I/I) periods (MIS 5c, MIS 5a, MIS 3) and the Holocene, and the blue shadow indicates the glacial/stadial (G/S) periods (MIS 5d, MIS 5b, MIS 4, MIS 2). The dashed lines indicate the three end-member mixing curves, and the solid lines indicate the quantification of the volcanic member. (For interpretation of the references to colour in this figure legend, the reader is referred to the web version of this article.)

the study site (Nürnberg and Tiedemann, 2004; Zou et al., 2015), as the Okhotsk Sea is situated in the downwind zone of the westerlies, potentially causing it to receive dusts transported by the westerlies. Previous research indicated that the westerlies were intensified during cold periods and weakened during warm periods (Hovan and Rea, 1991). This phenomenon facilitated the dust supply from the Asian interiors to the Okhotsk Sea during cold intervals (Porter and An, 1995; Vandenberghe et al., 2006; Fig. 7A). However, in comparison to the sediment discharge from the Amur River and the strengthened sea-ice drift during the G/S periods in the Okhotsk Sea, the contribution of dust is significantly constrained (Wang et al., 2017), given the low dust flux of approximately 2 $g/m^2/yr$ to the modern Okhotsk Sea (Uematsu et al., 2003; Yasuda et al., 2014). Consequently, the Amur River and Sakhalin Island, as well as the Okhotsk-Chukotka volcanic belt and the southern Kuril Islands/Hokkaido, are the main source areas, with only a limited dust contribution from the Asian continent during cold periods.

The foregoing interpretation of provenance changes based on the εNd values is supported by the Th/Sc ratios (Fig. 8E). Th tends to be enriched in felsic rocks and thus it reflects the influence of terrigenous materials from the Amur River and Sakhalin Island, while Sc typically occurs in mafic rocks, reflecting the input of volcanic materials (Taylor and McLennan, 1985; Fig. 8E). Thus, the Th/Sc ratio can reflect the relative contributions of volcanic and continental materials in this region. It was reported that the Th/Sc values in the Okhotsk-Chukotka volcanic belt ranged between ~0.17 and ~ 0.24 (Tschegg et al., 2011), while they were significantly higher in the Amur River (~0.9–1.4; Sorokina and Zarubina, 2011). Therefore, decreases in the Th/Sc values indicated the increased contribution of materials from the Okhotsk-Chukotka volcanic belt and the southern Kuril Islands/Hokkaido during the I/I periods, whereas the increased Th/Sc values during the G/S periods indicated the increased contribution of terrigenous materials from the Amur River and Sakhalin Island.

5.2. Dynamics of sediment transport in the southwestern Okhotsk Sea and its environmental implications

The process of sediment transportation in the Okhotsk Sea is complicated due to the variable land-sea interaction dynamics in this region, and the diverse transport processes and mechanisms that include sea ice, ocean currents, and rivers (Derkachev et al., 2004; Nakatsuka et al., 2002; Yasuda et al., 2014; Wang et al., 2014, 2017; Zou et al., 2015). Studies of the sedimentary mineralogy, geochemistry, and biomarkers in the sediments of the Okhotsk Sea have revealed that sea-ice drifting is the dominant transport mechanism of coarse-grained materials during cold intervals with extensive sea-ice coverage (Goldberg et al., 2005; Gorbarenko et al., 2002; Katsuki et al., 2010; Nürnberg et al., 2011; Ternois et al., 2001; Wang et al., 2014, 2017; Zou et al., 2015). In contrast, surface ocean currents can transport fine-grained materials to the study site (Derkachev et al., 2004), while suspended particulate material from the Amur River and the Sakhalin Bay can be transported to the core site through the dense shelf water (DSW) and OSIW (Nakatsuka et al., 2002; Yasuda et al., 2014).

The transportation of medium-coarse grained sediments in the Okhotsk Sea is primarily via sea-ice drifting (Gorbarenko et al., 2002; Sakamoto et al., 2005; Vasilenko et al., 2017, 2019; Wang et al., 2014, 2017). However, during intervals of mild sea-ice condition (e.g. Holocene), this process plays a secondary role and surface ocean currents take precedence, facilitating the transport of fine-grained materials (Derkachev et al., 2004; Sakamoto et al., 2005), as a consequence of longer duration of ice-free period (Sakamoto et al., 2005). The pronounced increase in εNd values during the last deglacial/early Holocene transition (Fig. 8F) aligns with a notable decrease in EM3 and an abrupt increase in sea surface temperature (SST; Lo et al., 2018), indicating milder sea ice condition (Vasilenko et al., 2019). Additionally, an abrupt increase in grain size component EM1 indicates the enhanced influence of surface ocean currents (Fig. 8B–D). A pronounced shift from a bimodal grain-size distribution to a unimodal distribution occurred at

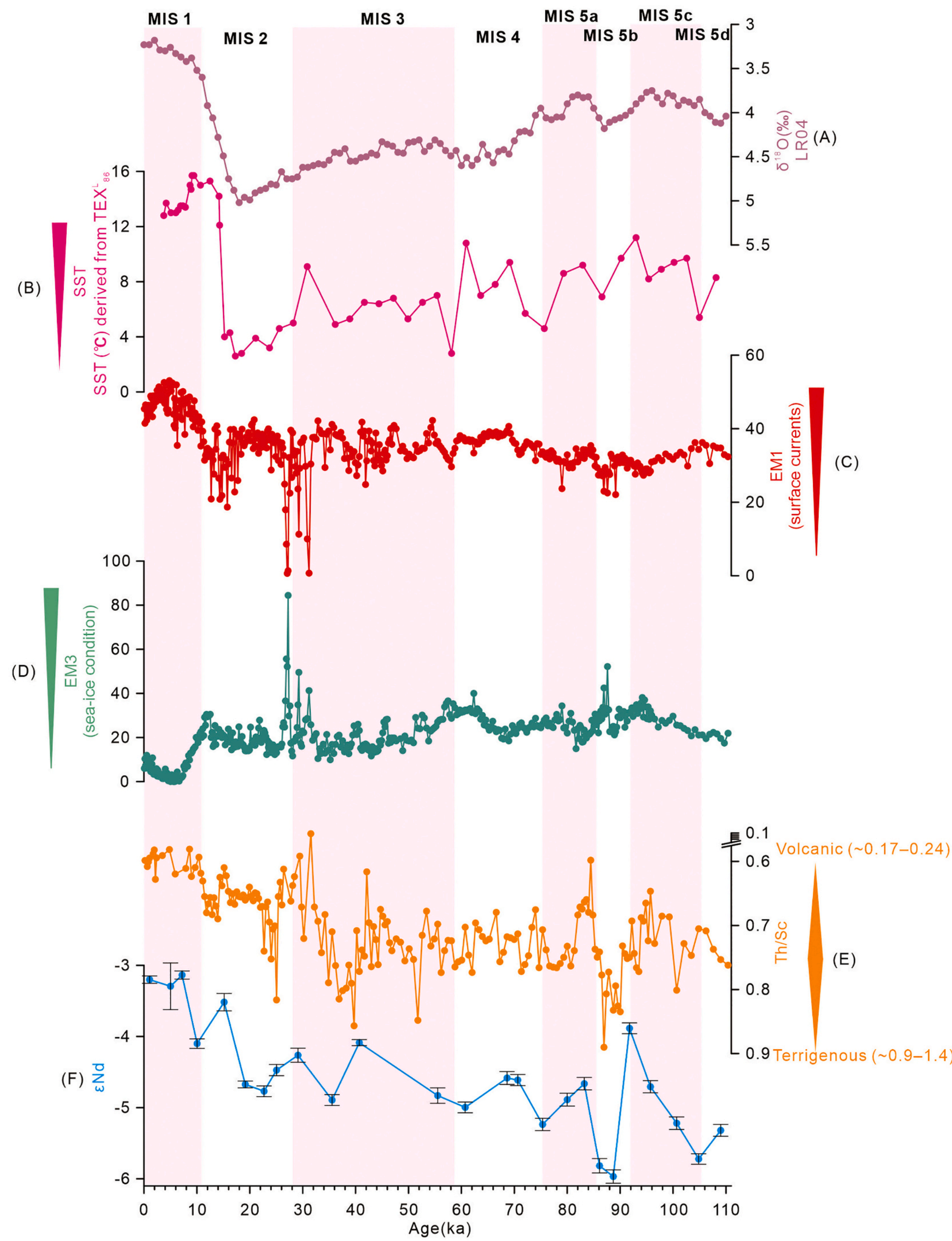

Fig. 8. Comparison of geochemical records from LV55-40-1 with global and regional records since the last interglacial period. (A) LR04 marine oxygen isotope stack (Lisiecki and Raymo, 2005) with marine isotope stages (MIS) indicated, (B) Sea surface temperature (SST, °C) derived from TEX$^{L}_{86}$ in core MD01-2412 (Lo et al., 2018), (C) Grain-size EM1, representing changes in surface currents change, (D) grain-size EM3, representing sea ice variations, (E) Th/Sc ratios, and (F) εNd values with 2σ error bars. The end-member values of δEu and Th/Sc for volcanic rocks are from Tschegg et al. (2011), and those for terrigenous materials are from Sorokina and Zarubina (2011). The εNd values (1.74 and 4.74) and $^{87}Sr/^{86}Sr$ ratios (0.706640 and 0.704441), corresponding to the volcanic layers at ~27.4 ka and ~ 31.5 ka, are not shown in the figure. The pink bars represent the interglacial/interstadial (I/I) periods (MIS 5c, MIS 5a, MIS 3) and the Holocene. (For interpretation of the references to colour in this figure legend, the reader is referred to the web version of this article.)

~8 ka (Fig. 4C, D), which suggests a transition from sea-ice drifting to the dominance of surface ocean currents in sediment transport during the Holocene. With the enhanced chemical weathering volcanic input from the Okhotsk-Chukotka volcanic belt and the southern Kuril Islands/Hokkaido during the Holocene (Dessert et al., 2001, 2009; Zhong et al., 2021), even a minor addition of volcanic materials (characterized by the most radiogenic εNd values) from these regions could significantly impact the εNd values in the sediments of core LV55-40-1 (Fig. 9A).

The elevated abundance of grain-size component EM3 during the interval of MIS 5–2 suggests strengthened sea-ice activity compared with the Holocene (Fig. 8D); consequently, the subtle variations in provenance during these intervals are mainly attributed to variations in sea-ice drifting. Previous studies showed that sea-ice drifting in this region is primarily influenced by changes in winds, which are affected by changes in the atmospheric circulation driven by the Siberian High (SH) and Aleutian Low (AL; Gorbarenko et al., 2010; Kimura and Wakatsuchi, 2004; Vasilenko et al., 2019; Wang et al., 2017). During the G/S periods, the SH was strengthened and its center shifts to the eastern Asian continent, while the AL was weakened and its center shifts to the northeastern Pacific (Vasilenko et al., 2019; Fig. 9B). Hence, cold northwesterly winds prevailed at these times (Fig. 9B), leading to a sever sea-ice condition which is indicated by the high abundance of EM3 and low SST in this region (Lo et al., 2018; Vasilenko et al., 2019; Fig. 8B, D). Consequently, terrigenous materials on the northwestern shelf and along the eastern coast of Sakhalin Island were more easily transported to the study area by the prevailing northwesterly winds during the G/S periods (Fig. 9B).

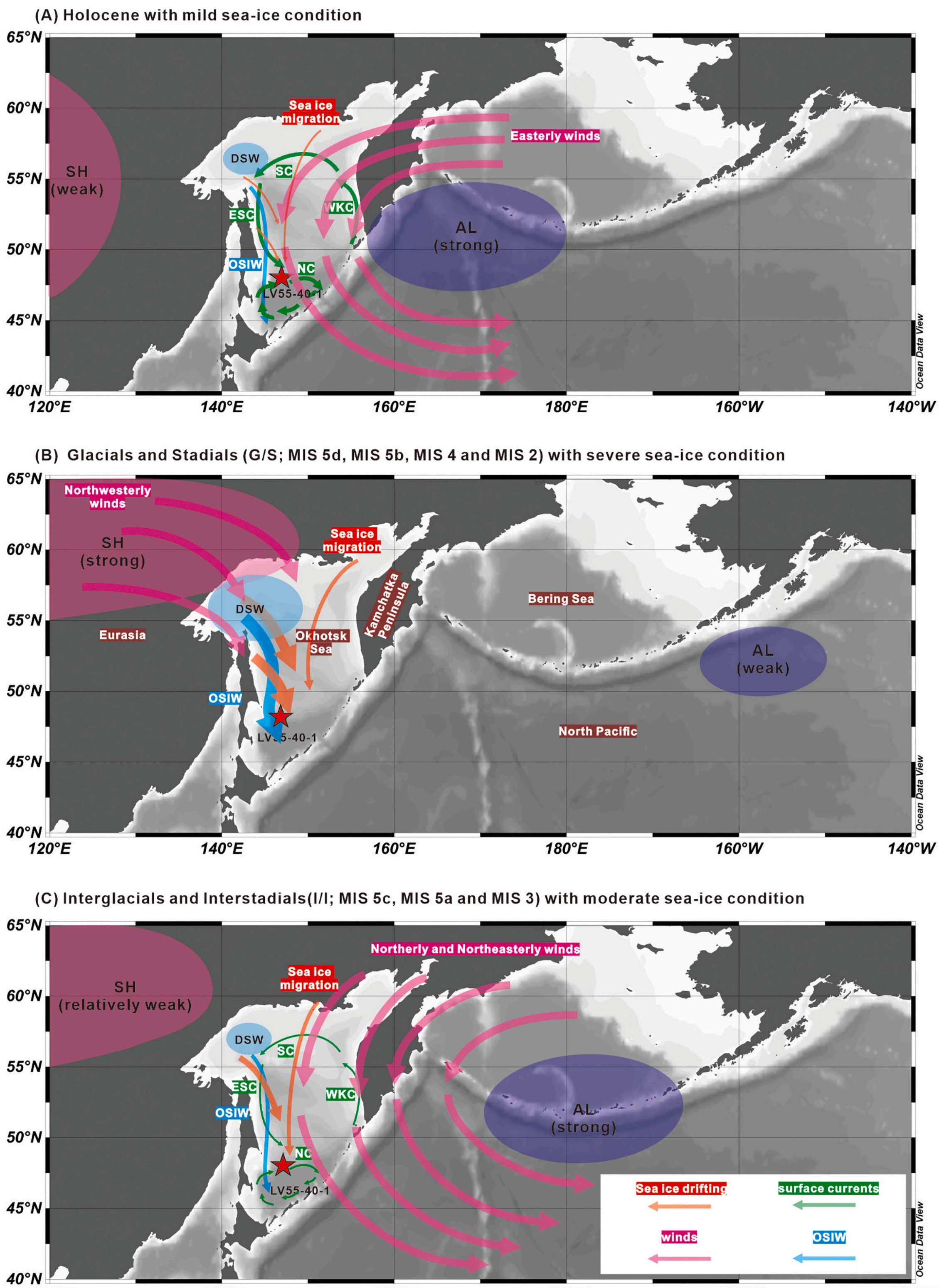

(caption on next page)

Fig. 9. Schematic illustration showing the influence of sea-ice drifting and ocean currents on the sediment provenance of the Okhotsk Sea for different climatic conditions and atmospheric circulations. (A) During the Holocene, surface currents dominated the sediment transport. The prevailing easterly winds were influenced by the Siberian High (SH) weakened and shifted westward to the central Asian continent, while the AL strengthened and moved eastward towards the eastern Kamchatka Peninsula (Vasilenko et al., 2019). (B) During the G/S periods, sea-ice drifting dominated the sediment transport. The SH strengthened and moved to the eastern Asian continent, while the AL weakened and its center shifted to the northeastern Pacific (Vasilenko et al., 2019). These changes resulted in the prevalence of northwesterly winds and promoted sea ice formation in the northwestern Okhotsk Sea which drifted to the southwestern Okhotsk Sea. The dense shelf water (DSW) and the Okhotsk Sea Intermediate Water (OSIW) strengthened and carried materials from the Amur River to the study area. (C) During the I/I periods. Sea-ice drifting dominated sediment transport while transport by surface currents was secondary. The SH was relatively weakened and retreated to the central Asian continent, while, the AL strengthened and its center moved to the south of the Aleutian Islands (Vasilenko et al., 2019). The resulting northerly and northeasterly winds favor sea-ice drifting from the northern and northeastern shelf of the Okhotsk Sea to the study area. Furthermore, surface currents transported more volcanic materials to the study site. The orange arrows represent the direction of sea-ice drifting; the green arrows represent the surface currents of the East Sakhalin Current (ESC), Sredinnoe Current (SC), West Kamchatka Current (WKC), and Northeast Current (NC); the pink arrows represent wind directions; and blue arrows represent the transportation of the DSW and OSIW. The line thickness is proportional to changes in intensity of transportation. (For interpretation of the references to colour in this figure legend, the reader is referred to the web version of this article.)

The cold northwesterly winds during the G/S periods also favored the development of polynyas in the northwestern coastal region of the Okhotsk Sea, which in turn persistently accelerated the formation of sea ice (Itoh, 2003; Wong et al., 1998). The enhanced sea-ice formation could significantly contribute to the dense water production on the northwestern shelf due to the brine rejection, leading to the enhanced formation of OSIW during the G/S periods (Gorbarenko et al., 2004, 2020; Keigwin, 1998; Okazaki et al., 2005; Wong et al., 1998; Zhong et al., 2021; Fig. 9B). It has been reported that DSW, which is the source water of the OSIW, carries a significant amount of resuspended fine materials from the Amur River and the Sakhalin Bay to the southern Okhotsk Sea along the eastern coast of Sakhalin Island (Nakatsuka, 2004; Yasuda et al., 2014). Thus, these fine particles can be transported southward to the site of core LV55-40-1 via the DSW and the OSIW (Nakatsuka et al., 2002), as core LV55-40-1 is located along the pathway of OSIW export to the North Pacific.

During the I/I periods, the SH was comparatively weakened relative to the G/S periods, and its center shifted to the central Asian continent, while the center of the strengthened AL shifted to the south of the Aleutian Islands (Vasilenko et al., 2019; Fig. 9C). Thus, northerly and northeasterly winds prevailed over the Okhotsk Sea (Fig. 9C), leading to moderate sea-ice conditions, as evidenced by the relatively low abundance of grain-size component EM3 and the high SST in this region (Lo et al., 2018; Vasilenko et al., 2019; Fig. 8B, D). Additionally, the εNd values were relatively high during mid-MIS 4, comparable to those during MIS 5a and MIS 3 (Fig. 8F). This phenomenon can be attributed to a shift in the prevailing winds from the northwest to the northeast at this time (Vasilenko et al., 2017, 2019), as evidenced by reduced sea-ice coverage under relatively high SSTs in the Okhotsk Sea (Lo et al., 2018; Wang et al., 2021a; Fig. 8B, D). In this case, sea ice was formed along the northern and northeastern shelf and then migrated towards the southwestern Okhotsk Sea (Kimura and Wakatsuchi, 2004; Fig. 9C). As a result, volcanic materials from the Okhotsk-Chukotka volcanic belt were transported to the study site via sea-ice drifting during the I/I periods, although its contribution was limited compared with that of the Amur River and Sakhalin Island. In addition to sea-ice drifting, the influence of surface currents was relatively intensified compared to the G/S periods under moderate sea-ice conditions (Vasilenko et al., 2019), as evidenced by the inverse variations of grain-size components EM1 and EM3 (Fig. 8C, D). The relatively enhanced surface currents played a crucial role in transporting fine-grained volcanic materials from the Okhotsk-Chukotka volcanic belt and the southern Kuril Islands/Hokkaido to the study area during these intervals.

6. Conclusions

We have investigated the Sr and Nd isotopic compositions of surface sediment samples and of the sediments of core LV55-40-1 from the southwestern Okhotsk Sea, to reconstruct variations in the provenance of terrigenous sediments over the past ~110 kyr. The changes in $^{87}Sr/^{86}Sr$ and εNd in core LV55-40-1 and in the surface sediments indicated that the Amur River and Sakhalin Island were the primary sources of sediments in the Okhotsk Sea (comprising ~60–80%), with minor contributions (~20–40%) from the Okhotsk-Chukotka volcanic belt and the southern Kuril Islands/Hokkaido. Our results reveal an overall increasing trend, characterized by an abrupt rise in εNd values in the early Holocene, together with secondary cyclic fluctuations in εNd values during the interval of MIS 5–2.

We infer that these provenance variations were primarily controlled by the competing forces of sea-ice drifting driven by atmospheric circulation patterns and by changes in ocean circulation. During the Holocene with mild sea-ice condition, sediment transport was mainly by surface currents which carried fine-grained volcanic materials from the Okhotsk-Chukotka volcanic belt and the southern Kuril Islands/Hokkaido to the study area.

Provenances changes during MIS 5–2 were dominated by sea-ice drifting. During the G/S periods, with severe sea-ice conditions, northwesterly winds prevailed and promoted the southeastward drift of sea ice formed along the northwestern shelf and the eastern coast of Sakhalin Island. This process carried abundant terrigenous materials from the Amur River and Sakhalin Island to the study area. Additionally, fine-grained material from the Amur River may have been transported by the OSIW to the study area during these periods. Conversely, during the I/I periods with moderate sea-ice conditions, northerly and northeasterly winds caused the drift of sea ice from the northern and northeastern shelf towards the southwestern Okhotsk Sea, and this resulted in the increased supply of volcanic materials from the Okhotsk-Chukotka volcanic belt. During the I/I periods, surface currents may also play important role in transporting materials from the Okhotsk-Chukotka volcanic belt and the southern Kuril Islands/Hokkaido to the study area.

CRediT authorship contribution statement

Anqi Wang: Writing – review & editing, Writing – original draft, Methodology, Data curation. **Zhengquan Yao:** Writing – review & editing, Project administration, Funding acquisition. **Xuefa Shi:** Writing – review & editing, Project administration, Funding acquisition. **Kunshan Wang:** Writing – review & editing, Investigation. **Yanguang Liu:** Writing – review & editing, Investigation, Funding acquisition. **Jianjun Zou:** Writing – review & editing, Investigation. **Yuriy Vasilenko:** Writing – review & editing, Investigation. **Fengdeng Shi:** Writing – review & editing, Investigation. **Zhi Dong:** Writing – review & editing, Funding acquisition. **Xiaojing Wang:** Methodology, Data curation. **Aimei Zhu:** Methodology, Conceptualization. **Zhengfan Lin:** Methodology, Data curation. **Xinqing Zou:** Writing – review & editing, Project administration. **Sergey Gorbarenko:** Writing – review & editing, Funding acquisition. **Alexander Bosin:** Writing – review & editing, Investigation.

Declaration of competing interest

The authors declare that they have no known competing financial interests or personal relationships that could have appeared to influence the work reported in this paper.

Data availability

The raw data are provided in Tables 1 and 2.

Acknowledgments

This work was jointly supported by the National Natural Science Foundation of China (42176088), the National Key Research and Development Program of China (Grant No. 2023YFF0804600), Laoshan Laboratory (LSKJ202204200), the Taishan Scholar Foundation of Shandong Province (tspd20181216), the Shandong Provincial Natural Science Foundation (Grant ZR2022QD005), the National Natural Science Foundation of China (Grant 42206065), the Russian Science Foundation, Russia (Grant No 22-17-00118), and the Russian state budget *121021700342-9* of the V.I. Il'ichev Pacific Oceanological Institute of Far East Branch of the Russian Academy of Sciences. We thank Prof. Jan Bloemendal for polishing the language.

References

Apt, Y.E., Akinin, V., Wright, J., 1998. Sr, Nd, and Pb isotopes in neogene melanephelinites and deep-seated xenoliths from Northeast Russia. Geochem. Int. 36 (1), 24–33.

Asahara, Y., Takeuchi, F., Nagashima, K., Harada, N., Yamamoto, K., Oguri, K., Tadai, O., 2012. Provenance of terrigenous detritus of the surface sediments in the Bering and Chukchi Seas as derived from Sr and Nd isotopes: implications for recent climate change in the Arctic regions. Deep-Sea Res. II 61–64, 155–171. https://doi.org/10.1016/j.dsr2.2011.12.004.

Chebykin, E.P., Gorbarenko, S.A., Stepanova, O.g.G., Panov, V.S., Goldberg, E.L., 2015. Geochemical multielement signatures of glacial and interglacial facies of the Okhotsk Sea deepwater sediments during the past 350 kyr: a response to global climate changes at the orbital and millennial scales. Paleoceanography. 30, 303–316. https://doi.org/10.1002/2014pa002718.

Chen, J., Zou, J., Zhu, A., Shi, X., Nürnberg, D., Lembke-Jene, L., Tiedemann, R., Wang, K., Wu, Y., Dong, Z., Liu, J., Dou, R., 2021. Geochemistry of Surface Sediments from the Emperor Seamount Chain, North Pacific. Front. Earth Sci. 9, 674842 https://doi.org/10.3389/feart.2021.674842.

Churikova, T., Dorendorf, F., WÖRner, G., 2001. Sources and fluids in the Mantle Wedge below Kamchatka, evidence from across-arc geochemical variation. J. Petrol. 42 (8), 1567–1593. https://doi.org/10.1093/petrology/42.8.1567.

Colin, C., Turpin, L., Blamart, D., Frank, N., Kissel, C., Duchamp, S., 2006. Evolution of weathering patterns in the Indo-Burman Ranges over the last 280 kyr: effects of sediment provenance on $^{87}Sr/^{86}Sr$ ratios tracer. Geochem. Geophys. Geosyst. 7 https://doi.org/10.1029/2005GC000962. Q03007.

Derkachev, A.N., Nikolaeva, N.A., Gorbarenko, S.A., 2004. The peculiarities of supply and distribution of clastogenic material in the Sea of Okhotsk during Late Quaternary (in Russian). Rus. J. Pac. Geo. 23 (1), 37–52.

Dessert, C., Dupré, B., Franßcois, L.M., Schott, J., Gaillardet, J., Chakrapani, G.J., Bajpai, S., 2001. Erosion of Deccan Traps determined by river geochemistry: impact on the global climate and the $^{87}Sr/^{86}Sr$ ratio of seawater. Earth Planet. Sci. Lett. 188 (3–4), 459–474. https://doi.org/10.1016/S0012-821X(01)00317-X.

Dessert, C., Gaillardet, J., Dupre, B., Schott, J., Pokrovsky, O.S., 2009. Fluxes of high- versus low-temperature water–rock interactions in aerial volcanic areas: Example from the Kamchatka Peninsula, Russia. Geochim. Cosmochim. Acta. 73 (1), 148–169. https://doi.org/10.1016/j.gca.2008.09.01.

Dou, Y., Yang, S., Liu, Z., Shi, X., Li, J., Yu, H., Berne, S., 2012. Sr-Nd isotopic constraints on terrigenous sediment provenances and Kuroshio Current variability in the Okinawa Trough during the late Quaternary. Palaeogeogr. Palaeoclimatol. Palaeoecol. 365–366, 38–47. https://doi.org/10.1016/j.palaeo.2012.09.003.

Dou, R., Zou, J., Shi, X., Zhu, A., Dong, Z., Zou, X., Gorbarenko, S., Achyuth, H., 2022. Provenance discrimination of siliciclastic sediments in the Western Sea of Japan over the past 30 kyr: evidence from Major, Trace elements, and Pb Isotopes. Lithosphere 2022 (Special 9). https://doi.org/10.2113/2022/6405238, 6405238.

Erel, Y., Harlavan, Y., Blum, J.D., 1994. Lead isotope systematics of granitoid weathering. Geochim. Cosmochim. Acta 58 (23), 5299–5306. https://doi.org/10.1016/0016-7037(94)90313-1.

Frank, M., 2002. Radiogenic isotopes: tracers of past ocean circulation and erosional input. Rev. Geophys. 40 (1) https://doi.org/10.1029/2000RG000094, 1-1–1-38.

Freeland, H.J., Bychkov, A.S., Whitney, F., Taylor, C., Wong, C.S., Yurasov, G.I., 1998. WOCE section P1W in the Sea of Okhotsk: 1. Oceanographic data description. J. Geophys. Res. Oceans 103 (C8), 15613–15623. https://doi.org/10.1029/98JC00368.

Goldberg, E.L., Gorbarenko, S.A., Shaporenko, A.D., Phedorin, M.A., Artemova, A.V., Bosin, A.A., Zolotarev, K.V., 2005. SRXFA for element compositions of bottom sediments from the Okhotsk Sea. Nucl. Inst. Methods Phys. Res. B 543 (1), 280–283. https://doi.org/10.1016/j.nima.2005.01.241.

Gorbarenko, S.A., Nürnberg, D., Derkachev, A.N., Astakhov, A.S., Southon, J.R., Kaiser, A., 2002. Magnetostratigraphy and tephrochronology of the Upper Quaternary sediments in the Okhotsk Sea: implication of terrigenous, volcanogenic and biogenic matter supply. Mar. Geol. 183 (1–4), 107–129. https://doi.org/10.1016/S0025-3227(02)00164-0.

Gorbarenko, S.A., Southon, J.R., Keigwin, L.D., Cherepanova, M.V., Gvozdeva, I.G., 2004. Late Pleistocene–Holocene oceanographic variability in the Okhotsk Sea: geochemical, lithological and paleontological evidence. Palaeogeogr. Palaeoclimatol. Palaeoecol. 209 (1–4), 281–301. https://doi.org/10.1016/j.palaeo.2004.02.013.

Gorbarenko, S.A., Harada, N., Malakhov, M.I., Vasilenko, Y.P., Bosin, A.A., Goldberg, E. L., 2010. Orbital and millennial-scale environmental and sedimentological changes in the Okhotsk Sea during the last 350 kyr. Glob. Planet. Chang. 72 (1–2), 79–85. https://doi.org/10.1016/j.gloplacha.2010.03.002.

Gorbarenko, S.A., Harada, N., Malakhov, M.I., Velivetskaya, T.A., Vasilenko, Y.P., Bosin, A.A., Derkachev, A.N., Goldberg, E.L., Ignatiev, A.V., 2012. Responses of the Okhotsk Sea environment and sedimentology to global climate changes at the orbital and millennial scale during the last 350 kyr Pt. II. Deep-sea Res 61–64, 73–84. https://doi.org/10.1016/j.dsr2.2011.05.016.

Gorbarenko, S.A., Yanchenko, E.A., Psheneva, O.g.Y., Harada, N., Bosin, A.A., Artemova, A.V., Vasilenko, Y.P., 2020. Orbital and millennial-scale environmental and hydrological changes of the central Okhotsk Sea over the last 136 kyr inferred from micropaleontological (radiolarian and benthic foraminifera), geochemical and lithological proxies and the mechanisms responsible for them. Quat. Sci. Rev. 247, 106569 https://doi.org/10.1016/j.quascirev.2020.106569.

Horikawa, K., Asahara, Y., Yamamoto, K., Okazaki, Y., 2010. Intermediate water formation in the Bering Sea during glacial periods: evidence from neodymium isotope ratios. Geology. 38 (5), 435–438. https://doi.org/10.1130/G30225.1.

Hovan, S.A., Rea, D.K., 1991. Late pleistocene continental climate and oceanic variability recorded in northwest. Paleoceanography 6 (3), 349–370. https://doi.org/10.1029/91PA00559.

Itoh, M., 2003. Distribution and formation of Okhotsk Sea Intermediate Water: an analysis of isopycnal climatological data. J. Geophys. Res. 108 (C8), 3258. https://doi.org/10.1029/2002jc001590.

Jacobsen, S.B., Wasserburg, G.J., 1980. Sm-Nd isotopic evolution of chondrites. Earth Planet. Sci. Lett. 50 (1), 139–155. https://doi.org/10.1016/0012-821X(80)90125-9.

Kameda, J., Kimura, G., Melinikov, O.A., Hayasaka, Y., Hashimoto, Y., Sakashima, T., Arai, T., Yoshino, T., Suzuki, N., 2000. Geology of northern Sakhalin, the relative convergence between the Eurrasia and North America plates. J. Geogr. 109 (2), 235–248. https://doi.org/10.5026/jgeography.109.2_235.

Katsuki, K., Khim, B.-K., Itaki, T., Okazaki, Y., Ikehara, K., Shin, Y., Yoon, H.I., Kang, C. Y., 2010. Sea-ice distribution and atmospheric pressure patterns in southwestern Okhotsk Sea since the last Glacial Maximum. Glob. Planet. Chang. 72 (3), 99–107. https://doi.org/10.1016/j.gloplacha.2009.12.005.

Keigwin, L.D., 1998. Glacial-age hydrography of the far northwest Pacific Ocean. Paleoceanography. 13 (4), 323–339. https://doi.org/10.1029/98PA00874.

Kimura, N., Wakatsuchi, M., 2004. Increase and decrease of sea ice area in the Sea of Okhotsk: Ice production in coastal polynyas and dynamic thickening in convergence zones. J. Geophys. Res. Oceans 109, C09S03. https://doi.org/10.1029/2003JC001901.

Lapko, V.V., Radchenko, V.I., 2000. Sea of Okhotsk. In: Sheppard, C.R.C. (Ed.), Seas at the Millennium: An Environmental Evaluation. Pergamon, Amsterdam, pp. 463–472.

Li, T., Xu, Z., Lim, D., Chang, F., Wan, S., Jung, H., Choi, J., 2015. Sr-Nd isotopic constraints on detrital sediment provenance and paleoenvironmental change in the northern Okinawa Trough during the late Quaternary. Palaeogeogr. Palaeoclimatol. Palaeoecol. 430, 74–84. https://doi.org/10.1016/j.palaeo.2015.04.017.

Lisiecki, L.E., Raymo, M.E., 2005. A Pliocene-Pleistocene stack of 57 globally distributed benthic $\delta^{18}O$ records. Paleoceanography 20, PA1003. https://doi.org/10.1029/2004PA001071.

Lo, L., Belt, S.T., Lattaud, J., Friedrich, T., Zeeden, C., Schouten, S., Smik, L., Timmermann, A., Cabedo-Sanz, P., Huang, J.-J., Zhou, L., Ou, T.-H., Chang, Y.-P., Wang, L.-C., Chou, Y.-M., Shen, C.-C., Chen, M.-T., Wei, K.-Y., Song, S.-R., Fang, T.-H., Gorbarenko, S.A., Wang, W.-L., Lee, T.-Q., Elderfield, H., Hodell, D.A., 2018. Precession and atmospheric CO_2 modulated variability of sea ice in the central Okhotsk Sea since 130,000 years ago. Earth Planet. Sci. Lett. 488, 36–45. https://doi.org/10.1016/j.epsl.2018.02.005.

Lupker, M., France-Lanord, C., Galy, V., Lavé, J., Kudrass, H., 2013. Increasing chemical weathering in the Himalayan system since the last Glacial Maximum. Earth Planet. Sci. Lett. 365, 243–252. https://doi.org/10.1016/j.epsl.2013.01.038.

Mahoney, J.B., 2005. Nd and Sr isotopic signatures of fine-grained clastic sediments: a case study of western Pacific marginal basins. Sediment. Geol. 182 (1–4), 183–199. https://doi.org/10.1016/j.sedgeo.2005.07.009.

Martynov, Y.A., Kimura, J.I., Khanchuk, A.I., Rybin, A.V., Chashchin, A.A., Martynov, A. Y., 2007. Magmatic sources of quaternary lavas in the Kuril island arc: new data on Sr and Nd isotopy. Dokl. Earth Sci. 417, 1206–1211. https://doi.org/10.1134/S1028334X07080168.

McCave, I.N., 2008. Size sorting during Transport and deposition of fine sediments: sortable silt and flow speed. In: Rebesco, M., Camerlenghi, A. (Eds.), Developments in Sedimentology. Elsevier, Amsterdam, pp. 121–142.

McLennan, S.M., 1989. Rare earth elements in sedimentary rocks: Influence of provenance and sedimentary processes. Rev. Mineral. Geochem. 21, 169–200.

Meade, R.H., 1996. River-sediment inputs to major deltas. In: Milliman, J., Haq, B. (Eds.), Sea-Level Rise and Coastal Subsidence. Kluwer, London, pp. 63–85.

Morley, J.J., Hays, J.D., 1983. Oceanographic conditions associated with high abundances of the radiolarian Cycladophora davisiana. Earth Planet. Sci. Lett. 66, 63–72. https://doi.org/10.1016/0012-821X(83)90126-7.

Nakatsuka, T., 2004. Biogenic and lithogenic particle fluxes in the western region of the Sea of Okhotsk: Implications for lateral material transport and biological productivity. J. Geophys. Res. Oceans 109, C09S13. https://doi.org/10.1029/2003JC001908.
Nakatsuka, T., Yoshikawa, C., Toda, M., Kawamura, K., Wakatsuchi, M., 2002. An extremely turbid intermediate water in the Sea of Okhotsk: implication for the transport of particulate organic matter in a seasonally ice-bound sea. Geophys. Res. Lett. 29 (16) https://doi.org/10.1029/2001gl014029, 4–1–4–4.
Norman, M., Deckker, P., 1990. Trace metals in lacustrine and marine sediments: a case study from the Gulf of Carpentaria, northern Australia. Chem. Geol. 82, 299–318. https://doi.org/10.1016/0009-2541(90)90087-N.
Nürnberg, D., Tiedemann, R., 2004. Environmental change in the Sea of Okhotsk during the last 1.1 million years. Paleoceanography. 19, PA4011. https://doi.org/10.1029/2004pa001023.
Nürnberg, D., Dethleff, D., Tiedemann, R., Kaiser, A., Gorbarenko, S.A., 2011. Okhotsk Sea ice coverage and Kamchatka glaciation over the last 350 ka — evidence from ice-rafted debris and planktonic δ^{18}O. Palaeogeogr. Palaeoclimatol. Palaeoecol. 310 (3–4), 191–205. https://doi.org/10.1016/j.palaeo.2011.07.011.
Oka, T., 1990. Outline of Sakhalin geography and geology and notes of Sakhalin geological excursion in 1989 (in Japanese). Rep. Geol. Surv. Hokkaido. 62, 101–122.
Okazaki, Y., Takahashi, K., Katsuki, K., Ono, A., Hori, J., Sakamoto, T., Uchida, M., Shibata, Y., Ikehara, M., Aoki, K., 2005. Late Quaternary paleoceanographic changes in the southwestern Okhotsk Sea: evidence from geochemical, radiolarian, and diatom records. Deep-Sea Res. II 52 (16–18), 2332–2350. https://doi.org/10.1016/j.dsr2.2005.07.007.
Parkinson, C.L., Comiso, J.C., Zwally, H.J., Cavalieri, D.J., Gloersen, P., Campbell, W.J., 1987. Arctic Sea Ice, 1973–1976: Satellite Passive-Microwave Observations. NASA, Washington.
Petelin, V.P., 1957. The mineralogy of sand-silt fraction of sediment of the Sea of Okhotsk (in Russian). Tr. Inst. Okeanol. 22, 77–138.
Porter, S.C., An, Z., 1995. Correlation between climate events in the North Atlantic and China during the last glaciation. Nature. 375, 305–308. https://doi.org/10.1038/375305a0.
Rycroft, M.J., 1995. Arctic and antarctic sea ice, 1978–1987: satellite passive-microwave observations and analysis. J. Atmos. Terr. Phys. 57 (4), 445. https://doi.org/10.1016/0021-9169(95)90010-1.
Sakamoto, T., Ikehara, M., Aoki, K., Iijima, K., Kimura, N., Nakatsuka, T., Wakatsuchi, M., 2005. Ice-rafted debris (IRD)-based sea-ice expansion events during the past 100 kyrs in the Okhotsk Sea. Deep-Sea Res. II 52 (16–18), 2275–2301. https://doi.org/10.1016/j.dsr2.2005.08.007.
Sakamoto, T., Ikehara, M., Uchida, M., Aoki, K., Shibata, Y., Kanamatsu, T., Harada, N., Iijima, K., Katsuki, K., Asahi, H., 2006. Millennial-scale variations of sea-ice expansion in the southwestern part of the Okhotsk Sea during the past 120 kyr: Age model and ice-rafted debris in IMAGES Core MD01-2412. Glob. Planet. Chang. 53 (1–2), 58–77. https://doi.org/10.1016/j.gloplacha.2006.01.012.
Savostin, L., Zonenshain, L., Baranov, B., 1983. Geology and Plate Tectonics of the Sea of Okhotsk. In: Hilde, T.W.C., Uyeda, S. (Eds.), Geodynamics of the Western Pacific-Indonesian Region. https://doi.org/10.1029/GD011p0189.
Serreze, M.C., Stroeve, J., Barrett, A.P., Boisvert, L.N., 2016. Summer atmospheric circulation anomalies over the Arctic Ocean and their influences on September Sea ice extent: a cautionary tale. J. Geophys. Res. Atmos. 121, 11,463–11,485. https://doi.org/10.1002/2016jd025161.
Shuto, K., Hirahara, Y., Ishimoto, H., Aoki, A., Jinbo, A., Goto, Y., 2004. Sr and Nd isotopic compositions of the magma source beneath North Hokkaido, Japan: comparison with the back-arc side in the NE Japan arc. J. Volcanol. Geotherm. Res. 134 (1–2), 57–75. https://doi.org/10.1016/j.jvolgeores.2004.01.001.
Sorokina, O.A., Zarubina, N.V., 2011. Chemical composition of the bottom sediments in the middle reaches of the Amur River. Russ. J. Pac. Geol. 5, 469–476. https://doi.org/10.1134/s1819714011050095.
Steiger, R.H., Jäger, E., 1977. Subcommission on geochronology: Convention on the use of decay constants in geo- and cosmochronology. Earth Planet. Sci. Lett. 36 (3), 359–362. https://doi.org/10.1016/0012-821X(77)90060-7.
Talley, L.D., 1991. An Okhotsk Sea water anomaly: implications for ventilation in the North Pacific. Deep-Sea Res. I 38, S171–S190. https://doi.org/10.1016/s0198-0149(12)80009-4.
Talley, L.D., 1993. Distribution and formation of north pacific intermediate water. J. Phys. Oceanogr. 23 (3), 517–537. https://doi.org/10.1175/1520-0485(1993)023<0517:Dafonp>2.0.Co;2.
Tanaka, T., Togashi, S., Kamioka, H., Amakawa, H., Kagami, H., Hamamoto, T., Yuhara, M., Orihashi, Y., Yoneda, S., Shimizu, H., Kunimaru, T., Takahashi, K., Yanagi, T., Nakano, T., Fujimaki, H., Shinjo, R., Asahara, Y., Tanimizu, M., Dragusanu, C., 2000. JNdi-1: a neodymium isotopic reference in consistency with LaJolla neodymium. Chem. Geol. 168 (3–4), 279–281. https://doi.org/10.1016/S0009-2541(00)00198-4.
Taylor, S.R., McLennan, S.M., 1985. The Continental Crust: Its Composition and Evolution. Blackwell Scientific, Oxford, p. 312.
Ternois, Y., Kawamura, K., Keigwin, L., Ohkouchi, N., Nakatsuka, T., 2001. A biomarker approach for assessing marine and terrigenous inputs to the sediments of Sea of Okhotsk for the last 27,000 years. Geochim. Cosmochim. Acta 65 (5), 791–802. https://doi.org/10.1016/s0016-7037(00)00598-6.
Tschegg, C., Ntaflos, T., Akinin, V.V., 2011. Polybaric petrogenesis of Neogene alkaline magmas in an extensional tectonic environment: Viliga Volcanic Field, Northeast Russia. Lithos. 122 (1–2), 13–24. https://doi.org/10.1016/j.lithos.2010.11.009.
Turner, J., Hosking, J.S., Marshall, G.J., Phillips, T., Bracegirdle, T.J., 2015. Antarctic Sea ice increase consistent with intrinsic variability of the Amundsen Sea Low. Clim. Dyn. 46, 2391–2402. https://doi.org/10.1007/s00382-015-2708-9.
Tütken, T., Eisenhauer, A., Wiegand, B., Hansen, B.T., 2002. Glacial–interglacial cycles in Sr and Nd isotopic composition of Arctic marine sediments triggered by the Svalbard/Barents Sea ice sheet. Mar. Geol. 182 (3–4), 351–372. https://doi.org/10.1016/S0025-3227(01)00248-1.
Uematsu, M., Wang, Z., Uno, I., 2003. Atmospheric input of mineral dust to the western North Pacific region based on direct measurements and a regional chemical transport model. Geophys. Res. Lett. 30, 1342. https://doi.org/10.1029/2002gl016645.
Vandenberghe, J., Renssen, H., van Huissteden, K., Nugteren, G., Konert, M., Lu, H., Dodonov, A., Buylaert, J.-P., 2006. Penetration of Atlantic westerly winds into Central and East Asia. Quat. Sci. Rev. 25 (17–18), 2380–2389. https://doi.org/10.1016/j.quascirev.2006.02.017.
Vasilenko, Y.P., Gorbarenko, S.A., Bosin, A.A., Shi, X., Chen, M.-T., Zou, J., Liu, Y., Artemova, A.V., Yanchenko, E.A., Savenko, M.P., 2017. Millennial mode of variability of sea ice conditions in the Okhotsk Sea during the last glaciation (MIS 4–MIS 2). Quat. Int. 459, 187–200. https://doi.org/10.1016/j.quaint.2017.09.039.
Vasilenko, Y.P., Gorbarenko, S.A., Bosin, A.A., Artemova, A.V., Yanchenko, E.A., Shi, X., Zou, J., Liu, Y., Toropova, S.I., 2019. Orbital-scale changes of sea ice conditions of Sea of Okhotsk during the last glaciation and the Holocene (MIS 4–MIS 1). Palaeogeogr. Palaeoclimatol. Palaeoecol. 533, 109284 https://doi.org/10.1016/j.palaeo.2019.109284.
Wang, K., Shi, X., Wu, Y., Zou, J., Jiang, X., 2014. Characteristics and provenance imolications of heavy mineral in core OS03-1 from the east-southern Okhotsk Sea (in Chinese). Acta Oceanol. Sin. 36, 177–185. https://doi.org/10.3969/j.issn.0253-41932014 05.020.
Wang, K., Shi, X., Zou, J., Kandasamy, S., Gong, X., Wu, Y., Yan, Q., 2017. Sediment provenance variations in the southern Okhotsk Sea over the last 180 ka: evidence from light and heavy minerals. Palaeogeogr. Palaeoclimatol. Palaeoecol. 479, 61–70. https://doi.org/10.1016/j.palaeo.2017.04.017.
Wang, A., Yao, Z., Shi, X., Wang, K., Zou, J., Liu, Y., Wu, Y., Gorbarenko, S.A., 2021a. Orbital and millennial variations in sea ice in the Southwestern Okhotsk Sea since the last interglacial period and their implications. Front Earth Sci. 9, 710797 https://doi.org/10.3389/feart.2021.710797.
Wang, K., Shi, X., Zou, J., Liu, Y., Yao, Z., Gorbarenko, S.A., 2021b. Spatial distribution and provenance of detrital minerals of surface sediment in the Okhotsk Sea. Front Earth Sci. 9, 636850 https://doi.org/10.3389/feart.2021.636850.
Weltje, G.J., 1997. End-member modeling of compositional data: Numerical-statistical algorithms for solving the explicit mixing problem. Math. Geol. 29, 503–549. https://doi.org/10.1007/BF02775085.
Wong, C.S., Matear, R.J., Freeland, H.J., Whitney, F.A., Bychkov, A.S., 1998. WOCE line P1W in the Sea of Okhotsk: 2. CFCs and the formation rate of intermediate water. J. Geophys. Res. Oceans 103 (C8), 15625–15642. https://doi.org/10.1029/98jc01008.
Xie, Y., Kang, C., Chi, Y., Du, H., Wang, J., Sun, L., 2019. The loess deposits in Northeast China: the linkage of loess accumulation and geomorphic-climatic features at the easternmost edge of the Eurasian loess belt. J. Asian Earth Sci. 181, 103914 https://doi.org/10.1016/j.jseaes.2019.103914.
Yang, J., Honjo, S., 1996. Modeling the near-freezing dichothermal layer in the Sea of Okhotsk and its interannual variations. J. Geophys. Res. Oceans 101 (C7), 16421–16433. https://doi.org/10.1029/96jc01091.
Yao, Z., Shi, X., Guo, Z., Li, X., Nath, B.N., Betzler, C., Zhang, H., Lindhorst, S., Miriyala, P., 2023. Weakening of the South Asian summer monsoon linked to interhemispheric ice-sheet growth since 12 Ma. Nat. Commun. 14, 829. https://doi.org/10.1038/s41467-023-36537-6.
Yasuda, I., 1997. The origin of the North Pacific Intermediate Water. J. Geophys. Res. Oceans 102 (C1), 893–909. https://doi.org/10.1029/96jc02938.
Yasuda, T., Asahara, Y., Ichikawa, R., Nakatsuka, T., Minami, H., Nagao, S., 2014. Distribution and transport processes of lithogenic material from the Amur River revealed by the Sr and Nd isotope ratios of sediments from the Sea of Okhotsk. Prog. Oceanogr. 126, 155–167. https://doi.org/10.1016/j.pocean.2014.04.015.
Zhong, Y., Liu, Y., Gong, X., Wilson, D.J., Lu, Z., Liu, J., Song, T., Gorbarenko, S.A., Shi, X., Yang, X., Liu, Q., 2021. Coupled impacts of atmospheric circulation and sea-ice on Late pleistocene terrigenous sediment dynamics in the subarctic Pacific Ocean. Geophys. Res. Lett. 48 https://doi.org/10.1029/2021gl095312 e2021GL095312.
Zou, J., Shi, X., Zhu, A., Chen, M.-T., Kao, S., Wu, Y., Selvaraj, K., Scholz, P., Bai, Y., Wang, K., Ge, S., 2015. Evidence of sea ice-driven terrigenous detritus accumulation and deep ventilation changes in the southern Okhotsk Sea during the last 180 ka. J. Asian Earth Sci. 114, 541–548. https://doi.org/10.1016/j.jseaes.2015.07.020.
Zou, J., Shi, X., Zhu, A., He, L., Kandasamy, S., Tiedemann, R., Lembke-Jene, L., Shi, F., Gong, X., Liu, Y., Ikehara, M., Yu, P.-S., 2021. Paleoenvironmental implications of Sr and Nd isotopes variability over the past 48 ka from the southern Sea of Japan. Mar. Geol. 432, 106393 https://doi.org/10.1016/j.margeo.2020.106393.